Please cite the Published Version

Electrochemical overview: A summary of $ACo_xMn_yNi_zO_2$ and metal oxides as versatile cathode materials for metal-ion batteries

Jessica L. Pimlott Ryan J. Street, Michael P. Down *
and Craig E. Banks *

Faculty of Science and Engineering, Manchester Metropolitan University, Chester Street, Manchester M1 5GD, UK.

: To whom correspondence should be addressed.
Email: c.banks@mmu.ac.uk, Tel: ++(0)1612471196;
M.Down@mmu.ac.uk Tel: ++(0)1612471171;

Abstract

Early LiCoO$_2$ research provided the basis for the tremendous commercial success of Li$^+$ batteries since their invention in the early 1990s. Today, LiNiMnCoO$_2$ (Li-NMC) is one of the most widely used batteries in the rapidly evolving electronic vehicle industry. Metal-ion batteries continue to receive significant interest as research efforts aim to partially, or entirely, replace the use of scarcely available and toxic Co with elemental doping to form binary, ternary and quaternary layered oxides. Furthermore, safety concerns and rising uncertainty for the future of Li supplies have resulted in growing curiosity towards non-Li$^+$ rechargeable batteries such as Na$^+$ and K$^+$. A plethora of Co, Mn and Ni-containing layered oxides that achieve high capacities with good stability within Li+ batteries have been reported. Unfortunately, the success of Li$^+$ host materials does not always directly transfer to Na$^+$ and K$^+$ batteries due to the difficulty of reversibly intercalating larger ions without irreparably distorting the host structure.

Consequently, this report provides an overview of the Li-based materials surrounding the success of commercial Li-NMC and the subsequent progress of their lesser studied Na and K counterparts. The challenges for current cathode materials are highlighted, with opportunities for progression suggested. The summary presented in this review can be consulted to steer new and unique research avenues for layered oxide materials as metal-ion batteries cathodes.

Keywords: Na-ion batteries; K-ion batteries; Layered oxides.

1. Introduction

Since the commercialisation of Li^+ batteries in the early 1990s, Li^+ has dominated the energy storage industry due to its unparalleled energy density per weight.[1, 2] Consequently, the sharp increase in demand on finite Li supplies from the emerging electronic vehicle industry has caused concern for the future price and availability of Li.[3] In addition, the uneven distribution of Li deposits triggers political tension as the associated mining of Li^+ battery precursors often has ruinous environmental and sociological impacts.[4, 5] In order to ease the demand on finite Li supplies, research attention has switched to other alkali metals such as Na and K for use in metal-ion batteries.[6-12] Na^+ and K^+ batteries could partially alleviate the demand on Li by providing a sustainable accompanying technology to bear the burden of large-scale energy storage devices due to their natural abundance. Na and K are the sixth and eighth-most abundant elements in the earth's crust, respectively.[13-15] The precursor for Na^+ batteries, Na_2CO_3, is over 100-times cheaper than its Li^+ counterpart, Li_2CO_3 and is globally accessible.[14] Furthermore, the majority of Na_2CO_3 is obtained via a synthetic Solvay process, which is continually being developed into a greener process.[16]

Non-Li^+ batteries, such as Na- and K- ion, have numerous advantages. For example, from a cost perspective, Na^+ and K^+ batteries can utilise Al current collectors that are cheaper and lighter in weight than the Cu equivalents required for Li^+ batteries.[17, 18] Furthermore, they can safely be fully discharged to zero volts, whereas Li^+ batteries must remain at a minimum of around 30% state-of-charge to avoid dangerous thermal runaway.[19] This means that Na^+ and K^+ batteries can be transported and stored without the stringent safety regulations attached to Li^+ batteries. Due to their abundance and safety advantages, Na^+ batteries are starting to emerge onto the commercial market, alongside being a rewarding area of research.[7] However, progress is slower for K^+ batteries as it is challenging to find cathode materials that can accommodate the larger intercalating ions without irreversible distortion of the host structure. Many candidates for suitable cathodes have been investigated, one of the most popular being $A_xFe_yPO_4$, where A represents an alkali metal.[20-22]

$LiFePO_4$ is a commercial success for Li^+ cathodes. However, when applied to Na, the presence of electrochemically inactive mericite $NaFePO_4$ structures require complicated synthesis methods that are not easily translatable to industrial-scale manufacture.[23] Furthermore, $KFePO_4$ is electrochemically inactive in terms of K^+ intercalation, which requires complicated electrode design strategies to overcome.[24] This highlights the indirect knowledge transfer of

Li-based cathodes to other metal ion battery systems, emphasising the importance of individually investigating perspective battery cathodes towards each technology as a unique battery system. This surge in interest has given rise to a generation of layered transition metal oxide cathodes applied to a range of metal-ion batteries Li, Na[25, 26], K[27, 28], Mg[29], Zn[30, 31] and more.[32].

1.1. Layered transition metal oxides

First described by Delmas *et al*., the layered transition metal oxides have the general formula A_xMO_2, where A denotes an alkali metal (herein, Li, Na or K) and M denotes one or more transition metals of various oxidation numbers.[25, 30, 33, 34] The layered A_xMO_2 structure comprises repeating sheets of MO_6 octahedra, with the intercalating ions situated between these layers in either a prismatic or octahedral arrangement. This gives rise to two main phases, namely, P2- and O3-type layered oxides, where the number represents the number of unique layers in each unit cell. To form the O3 phase, with space grouping R-3m, the intercalating ions are positioned in an octahedral arrangement stacked in three distinct repeating layers. As described by Gonzalo *et al.* in terms of Na, this forms an $AB_{Na1}CA_{Na2}BC_{Na3}$ stacking pattern, where the Na shares one edge and one face with each MO_6 octahedra.[35] For the P2 equivalents with P6$_3$ mmc space grouping, the oxygen stacking forms a repeating $AB_{Na1}BA_{Na2}$ pattern. The Na is in a prismatic arrangement, where one shares a face plane with the MO_6 octahedra the other shares an edge. The MO_6 stacking pattern of the O3 and P2 layered structures are displayed in *Figure 1*. High-resolution transition electron microscopy (HR-TEM) images in *Figure 1*b reveal that the O3 and P2 phases coexist within the layered oxide material.

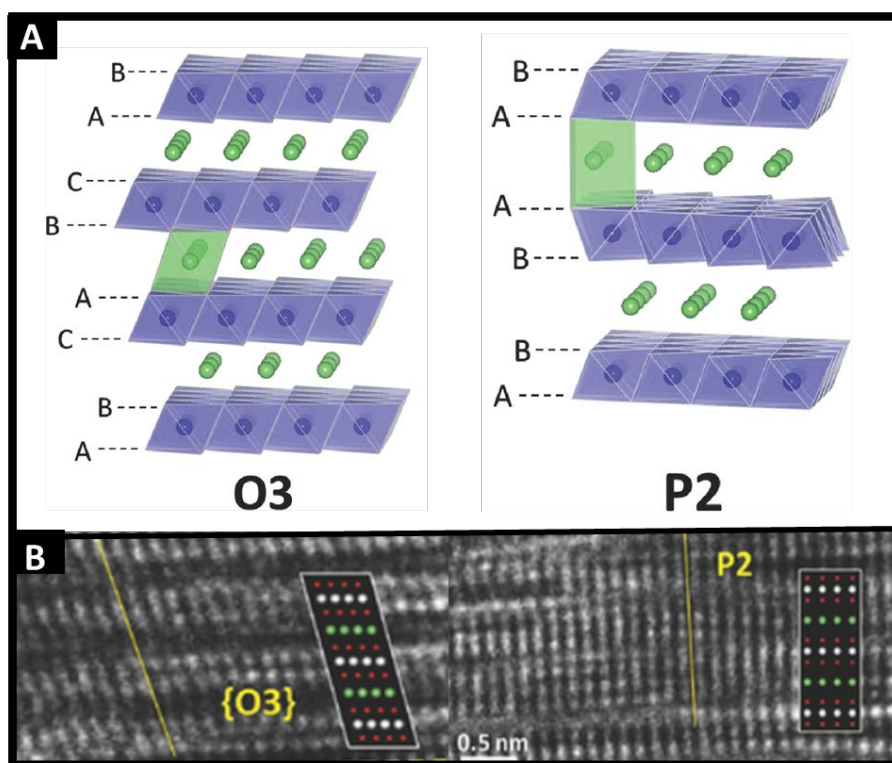*Figure 1. A) the stacking pattern of O3 and P2-A_xMO_2, where the blue spheres signify the transition metal atoms within the MO_6 layers, and the green spheres represent the intercalating metal ions. B) High-resolution transition electron microscopy of a ternary Na layered oxide material, showing the intergrowth of both the O3 and P2 crystal phases within the stacking pattern. Adapted from reference [36]*

Preliminary research by Mizushima *et al.* (published in 1980) demonstrated that Li^+ could reversibly be inserted into the layered rocksalt structure of $LiCoO_2$.[37] By the early 1990's $LiCoO_2$ emerged onto the commercial market, paving the way for the development of a plethora of layered transition metal oxide cathodes. Although $LiCoO_2$ still dominates much of the energy storage market in terms of portable electronics, there are still toxicity and price concerns about the prolonged use of Co-based cathodes. Kostiantyn *et al.* emphasise that Co supplies could fall short of demand as early as 2030 due to the scarcity of Co and lack of concentrated mineral deposits to facilitate a dependable supply.[38] This has kindled interest into binary and ternary materials that entirely or partially substitute Co. These include $LiMnO_2$[39-41], $LiCoMnO_2$[42, 43], and $LiMnNiO_2$[44-46]. The advantage of Mn inclusion is that it generally has less resistance due to the formation of spinel phases, whilst Ni provides high energy density. Therefore, $LiCo_xNi_yMn_zO_2$ (Li-NMC) was developed to yield the benefits of each transition metal oxide. Early reports of $LiCo_{0.33}Ni_{0.33}Mn_{0.33}O_2$ reveal high capacities over a wide voltage range, alongside good capacity retentions and high energy density.[47, 48] Furthermore, Li-NMC cathodes use significantly less Co than their $LiCoO_2$ equivalents. As such, these cathodes have gained commercial success, favoured by electronic vehicle manufacturers such as Nissan.[49]

Due to the success of Li-NMC in the electric vehicle industry placing a heavy demand on finite Li supplies, other alkali metals are investigated for their energy storage potentials. Although Na and K have energy storage capabilities, they are larger in atomic mass and ionic radius than Li, so they are better applied to stationary energy storage systems that favour safety and low cost than lightweight and high energy density. This is of particular interest to the rapidly developing renewable energy sector that relies on energy storage to mitigate their intermittent supply.

This overview discusses the cathode materials that proceeded commercial Li-NMC cathodes and assesses the progress of their Na^+ and K^+ counterparts. Herein, the ongoing research into the parent compounds of Li-NMC is discussed in terms of achievable capacity and capacity retentions, highlighting their limitations as an area for further research. Multiple methods of surface coating[50-52] and element doping[53-55] are discussed as methods of increasing the conductivity to enhance the already impressive electrochemical performance of Li-NMC cathode materials.[56]

2. Synthesis methods

Layered oxide materials are readily obtained from well-established, pioneering methods such as solid-state reactions,[57, 58] hydrothermal syntheses,[59, 60] co-precipitation procedures[61, 62] and the sol-gel method.[63, 64] Solid-state synthesis routes avoid complex, multi-step procedures and take advantage of easily obtained and relatively cheap carbonate and precursors whilst permitting the inclusion of dopants and phase variations by adjusting each precursor's stoichiometric amounts.[65] However, they require high calcination temperatures of between 800-1000°C over a prolonged duration. Compared to solid-state reactions and co-precipitation synthesis, sol-gel methods generally use lower synthesis temperatures while maintaining good crystallinity.[66] Whereas, Co-precipitation methods facilitate greater control over particle morphology but often rely on chelating agents such as ammonia.[67] Most recently, a freeze-drying method followed by a solid-state reaction achieved a Li-NMC material with uniform morphology, although the total synthesis time was around 60 hours.[68] Further work by Shi *et al.* then reduced the total synthesis time to 60 minutes by developing a complete microwave synthesis method.[69]

Innovation of synthesis methods has contributed to sustainability and, in some cases, increased electrochemical performance. For example, Su *et al.* reported synthesising a binary layered oxide via a hydrothermal method to expose the (100) crystal plane of the $NaMnO_2$ structure, subsequently facilitating faster reversible Na^+ extraction.[70] Whilst Shen *et al.* developed a co-precipitation method that uses lower ammonia concentration, thus producing less harmful by-products.[71] The constant innovation of synthesis procedures enables and improves the plethora of high-performance layered oxide materials detailed herein.

3. Single metal oxides

3.1. $ACoO_2$, where A = Li, Na, K

3.1.1. $LiCoO_2$

Simple Co-based metal oxides such as $LiCoO_2$ were amongst the first documented successes towards energy storage applications due to the unique cation ordering of the Co^{3+} and Li^+ ions that allows for easy lithium extraction from the rock salt structure. This feature is still explored over 40 years after initial Li^+ battery research.[37, 72-74] Although $LiCoO_2$ is widely utilised in commercial batteries, it only delivers around half of its theoretical capacity of 274 mAh g^{-1} as only 0.5 Li^+ can be extracted per formula unit.[52] One of the leading causes of capacity loss at high voltage ranges and increased temperatures is caused by migration of Co ions into the Li

7

layers, resulting in unwanted side reactions which reduce charging efficiency and contribute to the formulation of failure mechanisms such as dendrite or the Solid Electrolyte Interface, SEI, layer formation.[75] To address this issue, $LiCoO_2$ cathodes are often coated with Li^+ conducting materials such as Li_2ZrO_3,[52, 76, 77] Li_3PO_4,[78, 79] B_2O_3,[80] $LiNbO_3$[81] or doped with single elements such as halogens,[82] Al,[83] Ti,[84] and Zr[85] to name just a few.

At a relatively high voltage range of 3.0-4.5 V, an uncoated $LiCoO_2$ electrode retains a capacity of 105 mAh g^{-1} over 100 cycles, whilst an electrode coated with B_2O_3 retains a higher capacity of 153 mAh g^{-1}.[80] This results in capacity retentions of 63.4% and 84.4% for the uncoated and coated electrode respectively. Additionally, by coating a $LiCoO_2$ electrode with Li_2ZrO_3, the capacity retention is much higher at 85.2% over 100 cycles at a rate of 5 C.[52] Furthermore, with an upper cut-off voltage of +4.5 V, the capacity retention of an Al_2O_3 coated electrode was 95.0% over 80 cycles, this is more than double the capacity retention of 41.8% for the uncoated $LiCoO_2$ electrode.[51]

When charged and discharged at 55°C, the capacity of an uncoated $LiCoO_2$ electrode dropped from 109 mAh g^{-1} to 15.2 mAh g^{-1}; this results in poor capacity retention of 13.9%. In contrast, the $LiCoO_2$ electrode coated with Li_2ZrO_3 retains 71.3% of its capacity over 100 cycles under the same conditions [52] The coated sample also boasts an improved rate capability. The overall increase in the electrochemical performance is attributed to the synergistic effect of a synchronous lithiation route, illustrated in *Figure 2***Error! Reference source not found.**a, where the Li_2ZrO_3 coating and the $LiCoO_2$ bulk are formed simultaneously. XRD analysis confirms the migration of Zr^{4+} into the bulk $LiCoO_2$ and indicates that the Zr^{4+} are migrating into the transition metal sites and not replacing the Li^+ in the Li layers. The SEM images in *Figure 2*b-c show the spherical morphology of the $LiCoO_2/Li_2ZrO_3$ particles in the µm-nm range, whilst the high-resolution TEM images in *Figure 2*d-e reveal that the Li_2ZrO_3 layer has a uniform thickness of between 5 and 10 nm. The Li_2ZrO_3 coating forms a protective layer that inhibits detrimental phase transitions, avoids unwanted side reactions with the electrolyte, and promotes a homogenous SEI layer.
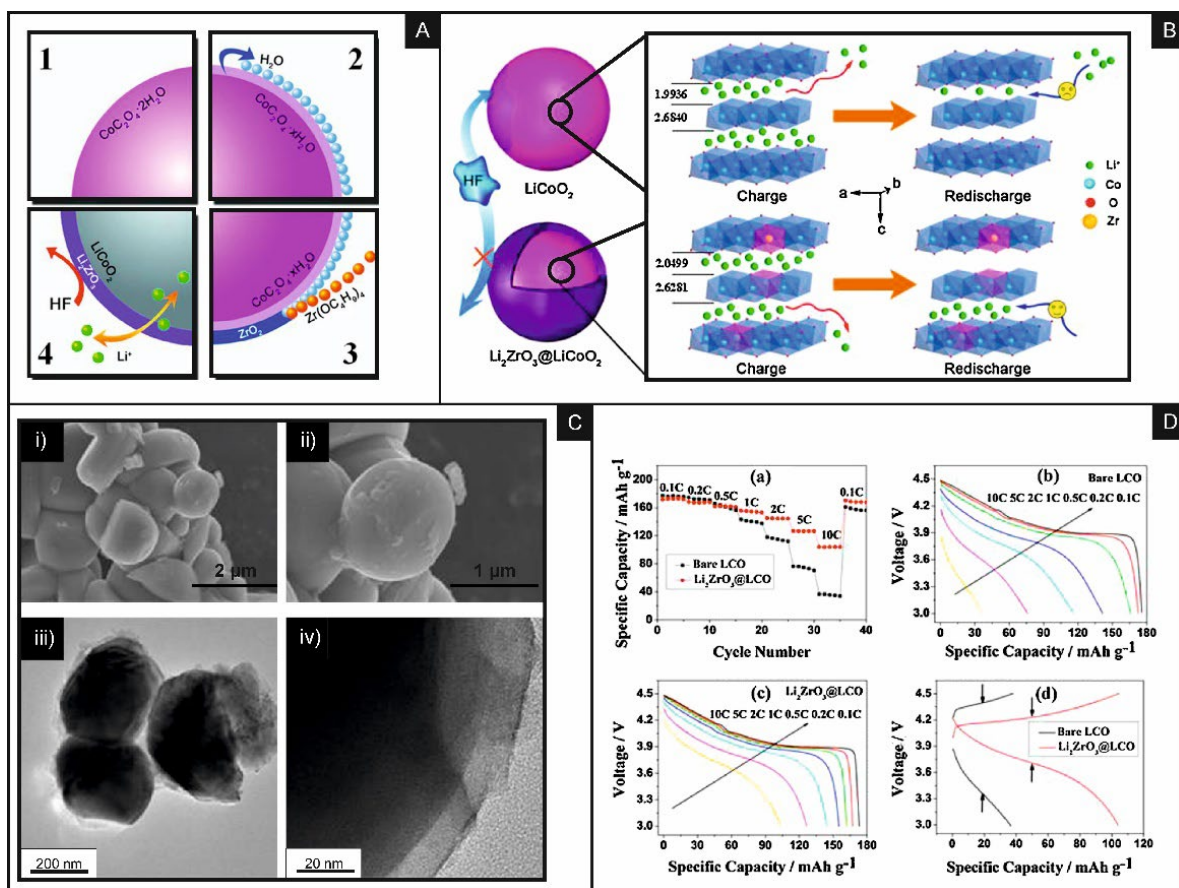
Figure 2. *A) schematic synthesis of the Li₂ZrO₃ coated samples, and B) the mechanism by which charging stability can be improved, illustrating the improved re-discharge properties due to increased crystalline spacing. C) SEM images of the Li₂ZrO₃ coated samples at i) low magnification and ii) High magnification. HR-TEM images of the sample samples at iii) low magnification and iv) high magnification. D) a) current handling performance for Li₂ZrO₃ modified LCO and blank LCO, b) galvanostatic charging behaviour of unmodified LCO, c) galvanostatic charging behaviour of Li₂ZrO₃ modified LCO c) a normalised comparison showing the significant improvement of the capacity and power handling capacity as a result of the modification. Figure adapted from[52]*

In a further attempt to avoid the capacity loss caused by structural transformations at high voltages, Hu *et al.* propose a hybrid Ti- and Ba-containing surface treatment in order to allow the reversibility of the phase transitions that occurs at 4.5 V.[86] Consequently, the modified electrode retains its structural integrity, with 90.3% capacity retention over 200 cycles in the voltage range of 3.0-4.5 V, compared to 72.4% for the uncoated electrode. Changing the morphology can influence the electrochemistry without the need for additional coatings or dopants. Xia *et al.* reveal a $LiCoO_2$ nanowire cathode that results in a relatively high discharge capacity of 135 mAh g^{-1} at 0.1 C in the limited voltage range of 3.0-4.2 V.[87] They attribute this to the mesoporous structure in a 3D "chain-like" structure, as shown in ***Figure 3***. This uncovers the potential of nanoscale $LiCoO_2$ materials as potential three-dimensional cathodes for micro-batteries due to their high power and energy density. Although $LiCoO_2$ cathode materials are already a commercial success, it is reported that there is a need to reduce reliance on dwindling Co reserves; later sections of this review highlight the importance of binary and ternary cathode systems in achieving this.[38]
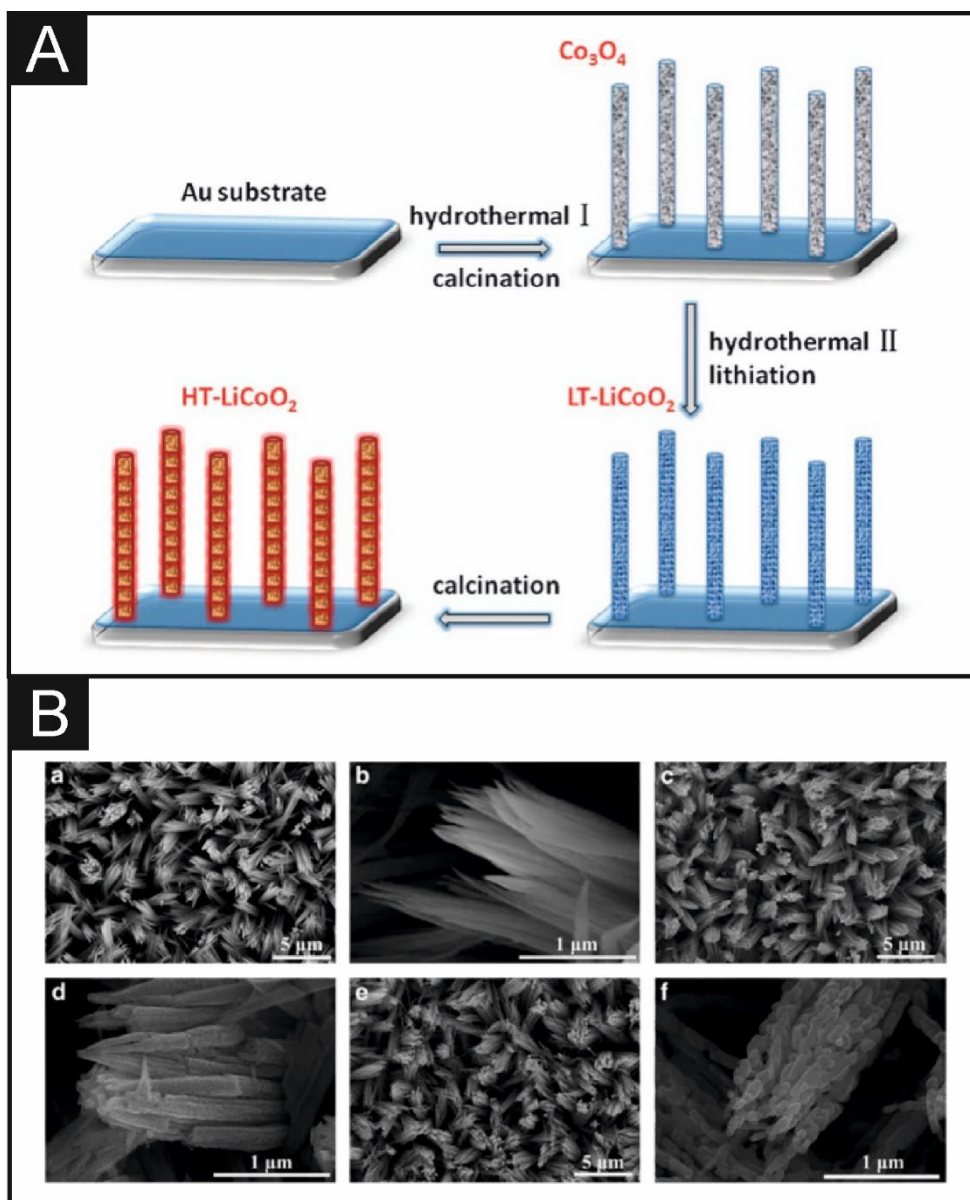
Figure 3. *A) synthesis approach for the manufacture of novel HT – LiCoO₂ "nanochains" the morphology of which, B) the resulting morphologies of the synthesis stage (a, b) Co₃O₄ nanowire arrays, (c, d) LT-LiCoO₂ nanowire arrays and (e, f) HT-LiCoO2 nanowire arrays. Figure adapted from* [87].

3.1.2. NaCoO$_2$

The vast applications of commercial LiCoO$_2$ have led to an interest in its Na-analogue, NaCoO$_2$. As is typical with layered oxides, the P2-type NaCoO2 is preferable to other phases due to its enhanced structural stability. The O3-type is often overlooked as it is more prone to the aforementioned phase transitions into distorted O3'- and P3 type phases, especially at higher cut-off voltages. Like LiCoO2, NaCoO2 is also susceptible to capacity loss from detrimental phase transitions and electrolyte-cathode reactions at high voltages and temperatures.

Low surface area architectures such as NaCoO$_2$ microspheres, the synthesis and morphology of which are shown in **Figure 4**, allow for a reduced contact area between the cathode and electrolyte, which is resulting in capacity retentions of between 86.0-95.0% over 300 cycles.[88, 89] This superior cycling stability is attributed to the enhanced ion transport efficiency of the mesoporous structure. The microsphere structure of this material, shown in **Figure 4**b, can also be replicated in the application of other Na$^+$ cathode materials such as NaFeO$_2$ and NaMnO$_2$.[89]

At higher cut-off voltages, the crystal structure of NaCoO$_2$ is thermally unstable after Na$^+$ extraction. This can cause the structure to degrade into Co oxides, ultimately resulting in loss of capacity. Hwang *et al.* observed the formation of the Co$_3$O$_4$ phase at a relatively low temperature of 100°C when an upper voltage of 4.5 V was used.[90] However, degradation to the Co$_3$O$_4$ phase was not observed until 400°C when the upper voltage was reduced to 3.5 V.
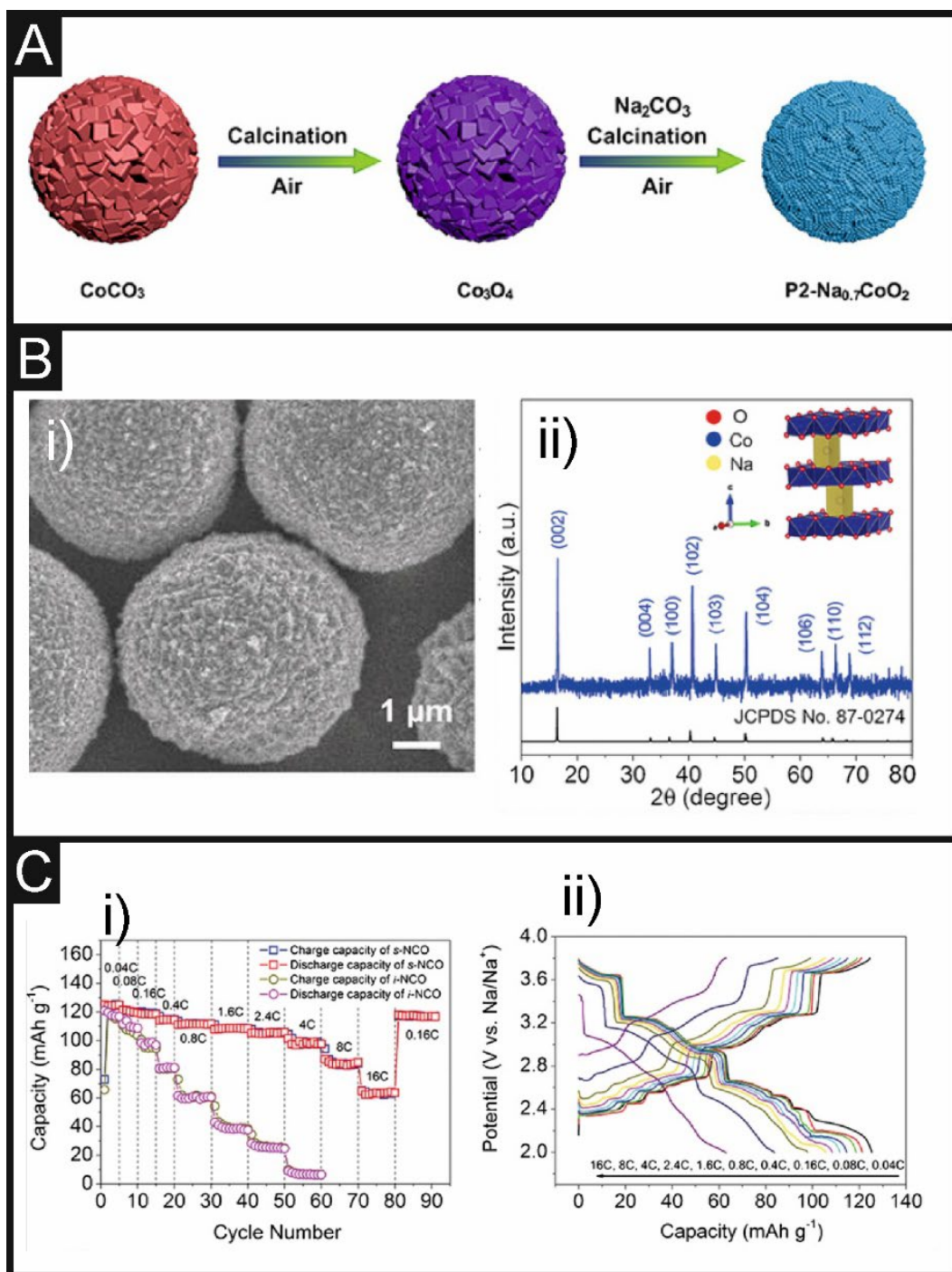
Figure 4. *A) Synthesis schematic for NaCoO₂ calcinated microspheres, B) i) the SEM of which and ii) XRD of the corresponding microstructures, highlighting the potential for high surface area microspheres with highly-ordered crystalline structures C) i) the current handling capability of the NaCoO₂ calcinated microspheres ii) the galvanostatic charge-discharge of the NaCoO₂ calcinated microspheres.*

3.1.3. KCoO$_2$

K$^+$ batteries are often overlooked for energy storage applications as some of the cathode materials that are successfully applied to Na$^+$ and K$^+$ batteries cannot facilitate intercalating the larger K$^+$ ions. The theoretical capacity of P2-K$_{0.6}$CoO$_2$ is considerably lower than LiCoO$_2$ at 60.0 and 274 mAh g^{-1}, respectively.[52, 91] Despite the larger size of the K ion, a self-templated KCoO$_2$ microsphere cathode achieves capacity retention of 87.0% over 300 cycles, with a reversible capacity of 71.0 mAh g^{-1}.[92] This is comparable to that of its NaCoO$_2$ microsphere equivalent that has a capacity of 86.5 mAh g^{-1} and capacity retentions of between 86.0-95.0%.[89] Furthermore, K ions can intercalate into the previously discussed NaCoO$_2$, achieving a K$^+$ battery with a reversible capacity of 82.0 mAh g^{-1} with a capacity retention of 80.0% over 50 cycles.[93] Comparatively higher than the capacity for K ions intercalated into untreated P2-K$_{0.6}$CoO$_2$, which yields a reversible capacity of 60.0 mAh g^{-1}.[94] It is difficult to achieve sustained reversible intercalation of K$^+$, as efforts usually result in electrodes that experience structural collapse upon deintercalation due to forced increase of interlayer distances by large K ions.[95] In general, when compared to Na$^+$, K$^+$ batteries generally achieve a lower capacity but compensate for this with a higher operational voltage due to the negative potential of K/K$^+$.[96] With further efforts to increase the achievable capacity, Co-based metal oxides could be promising K$^+$ cathode materials in terms of electrochemical performance. However, binary and ternary systems that use less Co should be encouraged to preserve finite Co reserves.

3.2. A$_x$MnO$_2$ where A = Li, Na, K

3.2.1. LiMnO$_2$

Although LiMnO$_2$ is a commercial success, it is susceptible to capacity loss that results from phase changes. Practically, an orthorhombic LiMnO$_2$ cathode achieves between 180 and 222 mAh g^{-1} of the 285 mAh g^{-1} theoretical capacity.[39, 40, 97] This is similar to 220 mAh g^{-1} for monoclinic LiMnO$_2$.[39] A combination of both orthorhombic and monoclinic phases, as demonstrated by Li *et al.* combines the high capacity of the monoclinic types with the enhanced stability of the orthorhombic type, as well as boasting the lowest impedance.[39] To avoid unwanted capacity loss, mesoporous structures are utilised to increase contact with the electrolyte and dampen the effects of volume increases within the structure. Exploiting this method, Tong *et al.* fabricated a mesoporous LiMnO$_2$ cathode that obtained a discharge capacity of 191 mAh g^{-1}, 85.0% of which was retained over 50 cycles at 0.5 C in the range of 2.0-4.4 V.[40] Cho *et al.* shows that the capacity retention can be improved to 98.0% over 50

14

cycles using an Al_2O_3 coating, which demonstrated no initial deterioration in its initial capacity, a property reportedly observed in metal oxide coatings, but this causes a low capacity of 30.0 mAh g^{-1}.[98] Cho *et al.* reported the improvement in capacity retention of the $LiCoO_2$ by sputtering a 10nm thick layer atop a $LiCoO_2$ thin film upon a platinum current collector. The performance remained significantly more stable for 100 cycles for current densities from 200 – 800 μA h/cm^2. It is observed that in the 3.0 V range, the presence of the Al coating limits the amount of Li that can be reversibly inserted.

Additionally, Nagasubramanian *et al.* used LiBO-coated $LiMnO_2$ to achieve a high capacity of 189 mAh g^{-1} with a capacity retention of 92.6%, a significant improvement from 172 mAh g^{-1} and 75.6% reported for the uncoated $LiMnO_2$ cathode.[99] However, the capacity decay at 3.0 V is still present. In contrast, the capacity retention can be improved up to 95.1% over 100 cycles at 0.1 C using Cr^{3+}/ Cr^{6+}-doping as reported by Chang *et al.*[100] A $Li_{1.27}Cr_{0.2}Mn_{0.53}O_2$ cathode achieves an initial discharge capacity of 195 mAh g^{-1}, which is close to the maximum theoretical capacity of 200 mAh g^{-1}. The enhanced performance is attributed to the faster Li^+ diffusion coefficient of 3.89×10^{-10} cm^2 s^{-1} after 100 cycles, which is notably higher than that of $Li_{1.2}Ni_{0.2}Mn_{0.2}O_2$ (1.63×10^{-12} cm^2 s^{-1}) and $Li_{1.23}Mn_{0.46}Ni_{0.15}Co_{0.16}O_2$ (2.78×10^{-15} cm^2 s^{-1}).[101]

3.2.2. NaMnO$_2$

Although Na_xMnO_2 materials exhibit high capacities nearing 200 mAh g^1, this capacity is often lost over the initial charge/discharge cycles due to strain from Mn^{3+} Jahn-Teller distortions.[102] Various attempts to mitigate the structural changes range from tailoring the morphology *via* modified solid-state synthesis[103-105], sol-gel methods,[106] hydrothermal methods,[107, 108] and more,[109-111] or using dopants such as Bi,[112] F,[113] and Fe.[114] Ferrara *et al.* observed an increase in capacity from 85.0 mAh g^{-1} to 95.0 mAh g^{-1} at a charge rate of 2 C by switching from a traditional solid-state synthesis method to an eco-friendly urea-based solution synthesis.[111] However, the capacity retention is limited to 75.7% over 200 cycles. Furthermore, Ma *et al.* demonstrated that $Na_{0.44}MnO_2$ nanorods formed using $MnCO_3$ derived from a hydrothermal synthesis method show higher capacity and capacity retention than those derived from co-precipitation methods.[108] A capacity of 140 mAh g^{-1} is delivered in the first discharge, alongside an impressive capacity retention of 98.2% over 40 cycles at 20 mA g^{-1}.

Nanoscale $Na_{0.44}MnO_2$ cathodes such as the nanorods mentioned above are commonly reported for discharge capacities as high as 140 mAh g^{-1}.[108, 110, 115] For example, well-shaped electrospun $Na_{0.44}MnO_2$ nanowires can be achieved from electrospinning and subsequent heat treatment

15

methods. The nanofibers were then subjected to heat-treatment at temperatures from 500-900°C. After thermal treatment at 900°C, it is shown that nanowires with dimensions ranging from 50 to 200 nm are achieved. Upon the extraction of 0.22 Na^+, a charge capacity of 66.7 mAh g^{-1} is observed, alongside a subsequent discharge capacity of 120 mAh g^{-1}.[110] The sample annealed at 900°C for 9 hours shows the optimal performance when compared to samples annealed for 6 hours and 12 hours, with a capacity retention of 97.3% over 200 cycles at 0.1 C. Post-mortem analysis determines that the morphology and crystal structure remain unchanged, showing excellent tolerance for Na^+ insertion and extraction. Furthermore, the material shows almost 100% capacity recovery when cycled from 0.1 C up to 50 C and back to 0.1 C. Combining the higher initial capacity of $O3-NaMnO_2$ with the enhanced stability of the $P2-NaMnO_2$ results in an electrode that can achieve a charge capacity of 171 mAh g^{-1}, dropping to 146 mAh g^{-1} after 50 cycles.[65] The capacity retention of 85.0% for $NaMnO_2$ in this instance is comparable to $LiMnO_2$ in a Li^+ battery at 84.9% over 50 cycles.[40, 65] Additionally, Zhang *et al.* synthesised $NaMnO_2$ that exists as a mix of monoclinic $NaMnO_2$ and $P2-NaMnO_2$, which results in a first discharge capacity of 195.6 mAh g^{-1}. However, this highlights the persisting stability issues as the capacity retention is only 52.0% over 30 cycles.[102]

In a full cell, a $Na_{0.44}MnO_2$ cathode combined with a water-based carboxymethyl cellulose binder and biowaste-derived hard carbon anode reaches a high Coulombic efficiency of 99.9% and a capacity of 109 mAh g^{-1} after 75 cycles at C/5.[105] However, extensive pre-sodination is required to combat the irreversible capacity and low Na content. To increase the stability, maximise the Coulombic efficiency and mitigate Na^+ deficiencies, Zheng *et al.* reveal a composite $Na_{0.44}MnO_2$ tunnel/$Na_2Mn_3O_7$ layered cathode that reaches a capacity of 278 mAh g^{-1} over a wide voltage range of 1.5-4.6 V at a charge rate of 20.0 mA g^{-1}.[116] For a $Na_{0.44}MnO_2$ cathode, 0.22 Na^+ is the maximum amount of Na that can be extracted without causing structural collapse, thus limiting the achievable capacity of pristine Mn-based cathodes.[105] For this reason, Na_xMnO_2 cathodes have been used as a foundation to develop binary and ternary Mn-based cathodes with enhanced electrochemical performance.

3.2.3. $KMnO_2$

$KMnO_2$ materials are less susceptible to ion migrations due to the larger ionic radius of the K^+ ions. Over 20 cycles, P3-type $K_{0.5}MnO_2$ retains 76% of its original 81.0 mAh g^{-1} capacity over 100 cycles, whereas $P3-K_{0.45}MnO_2$ retains 70.8% of 128.6 mAh g^{-1}.[27, 117] As the material can
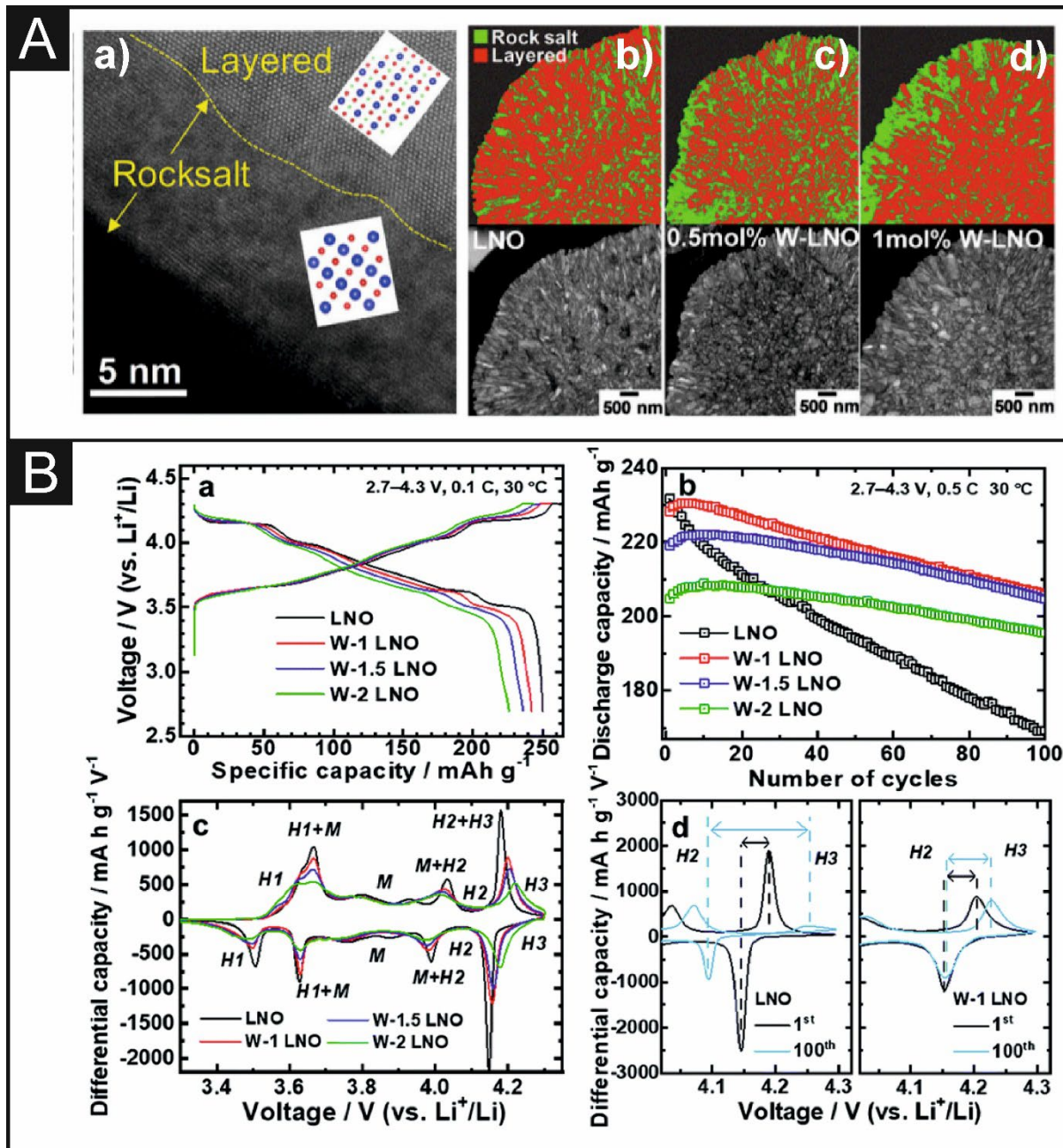
withstand phase transitions without breaking the Mn-O bonds, the structural changes are reversible, which minimises but does not fully mitigate the structural distortions.[95] Consequently, Chong *et al.* synthesised $K_{0.32}MnO_2$ nanosheets and confirmed *via* XRD analysis that irreversible structural changes are avoided over 100 cycles.[118] This results in 86.5% of the 95.1 mAh g^{-1} capacity remaining after 50 cycles at 10.0 mA g^{-1}. Xu *et al.* demonstrated that increasing amounts of Ti incorporated into the $KMnO_2$ structure has a detrimental effect on the capacity.[119] The capacity of $K_{0.56}Mn_{0.89}Ti_{0.11}O_2$ decreased from 138 to 85.6 with the increase of Ti to form $K_{0.56}Mn_{0.56}Ti_{0.44}O_2$. A potentially fruitful area of research may be to assess the impact of doping with electrochemically active elements that proved successful in $LiMnO_2$ batteries. Another avenue for increasing capacity is the use of birnessite nano-arrays. Lin *et al.* demonstrated that a $K_{0.77}MnO_2 \cdot 0.23H_2O$ cathode achieves an initial capacity of 134 mAh g^{-1} at 1 C.[120] At a higher charge rate of 10 C, a capacity of 77.0 mAh g^{-1} is delivered, 85.0 % of which is retained over 1000 cycles. This enhanced rate capability, capacity and stability arises from the high K content and inhibition of the structural decay facilitated by the birnessite structure.

3.3. A_xNiO_2 where A = Li, Na, K

3.3.1. $LiNiO_2$

$LiNiO_2$ received much interest in early battery research due to the relatively low cost and high theoretical capacity of 275 mAh g^{-1}.[121] However, early literature reported that $LiNiO_2$ was susceptible to unwanted side reactions and poor thermal stability.[122] At temperatures from 150°C, detrimental phase transitions to $LiNi_2O_4$ spinel-type phases were observed, as confirmed by TGA and DSC analysis.[123, 124] Thus, $LiNiO_2$ was limited to insufficient capacity as low voltage ranges minimise side reactions.[125] During charge/discharge cycles, the highly reactive Ni^{4+} on the surface is reduced to Ni^{2+}, forming a rock salt-structured layer on the electrode surface up to 20 nm in thickness.[126] Kim *et al.* uses a W dopant to stabilise the electrode by isolating the rock salt surface layer from the bulk, resulting in capacity retention of 90.0% over 100 cycles, opposed to 74.0% for the un-doped sample.[125] The surface segregation of the rock salt structure is demonstrated in *Figure 5*a-c by the (automatic TEM phase-identification/orientation mapping technique) ASTAR results, showing a clear distinction between the minor rock salt surface phase and the layered hexagonal structure of the bulk phase. It demonstrates that with increasing levels of W dopant, the more the rock salt layer is segregated at the particle surface. Furthermore, Ryu *et al.* used W-doping to increase the capacity retention to 95.5% over 100 cycles at 0.5 C, opposed to 73.7% for an un-doped

17

cathode, as shown in *Figure 5*d. This confirms the previous findings that a W-rich surface layer stabilises the $LiNiO_2$ cathode against unwanted phase transitions. It is vital to overcome the inherent stability issues that persist with binary $LiNiO_2$ cathodes, methods of which are discussed in detail by Bianchini *et al.*[126]

Figure 5. A) a)High-resolution TEM image displaying the surface after W coating (1.00% mol) with inset images showing a high-resolution Fourier images of the atomic arrangement. Automatic TEM phase-identification/orientation mapping and bright-field images of b) no coating, c) 0.50 mol% W coating and d) 1.00 mol% W coating. Adapted from [125]. B) Electrochemical performance at in the voltage range of 2.7-4.3 V for the pristine cathode, and coated with 1.00, 1.50, and 2.00 mol% W. a) voltage capacity profile, b) discharge capacity over 100 cycles, c and d) dQdV[-1] profiles differential capacity (vs. Li^{+}/Li), with d) emphasising phase transitions. Reproduced from [127]

3.3.2. NaNiO$_2$

With the revival of LiNiO$_2$, attention has been cast onto NaNiO$_2$ since it was first reported as a possible cathode material.[128] Monoclinic NaNiO$_2$ and orthorhombic Na$_2$NiO$_2$ boast impressive theoretical capacities of 236 and 392 mAh g^{-1}, respectively.[2] Na$_2$NiO$_2$ converts into NaNiO$_2$ during cycling; it is therefore proposed as an electrode additive to compensate for Na$^+$ loss at the negative electrode.[129] Vassilaras *et al.* revealed Na$_{0.85}$NiO$_2$ achieves a charge capacity of 199 mAh g^{-1}, then 0.62 Na$^+$ can be re-intercalated for Na$_{0.62}$NiO$_2$ to deliver a discharge capacity of 147 mAh g^{-1} in the 2.0-4.7 voltage range.[130] Cycling at a lower voltage range of 1.25-3.75 V results in lower charge and discharge capacities of 147 mAh g^{-1} and 123 mAh g$^{-1,}$ respectively. A proportion of charge capacity is due to the dissolution of Na$^+$ from the electrolyte, resulting in partial irreversibility. Wang *et al.* further explored the irreversibility of NaNiO$_2$ capacity, confirming that the detrimental phase transitions that occur below 3.0 V and above 4.0 V are mainly responsible for the irreversibility of Na$^+$ extraction.[131] In terms of capacity, NaNiO$_2$ is comparable to a NaCuO$_2$ cathode that achieves a reversible capacity of 190 mAh g^{-1} in the 0.75-4.2 V range.[132] This is less than the theoretical capacity of 235 mAh g^{-1} for NaNiO$_2$.

Despite showing good capacity retentions, the overall poor chemical and structural stability limits the potential of Ni-based single transition metal oxides. Kaushalya *et al.* suggest that doping NaNiO$_2$ cathodes with additional elements is essential to increase the *via*bility of Ni-based oxides towards Na$^+$ systems.[133] Based on theoretical predictions and elucidation of activation energies and solution enthalpies, Ga^{3+} is predicted to be the most promising dopant, although few examples exist of its use throughout literature as either a cathode or anode dopant.[134, 135]

3.3.3. KNiO$_2$

Parent components of KCo$_x$Ni$_y$Mn$_z$O$_2$ such as KCoO$_2$ and KMnO$_2$ cathodes are reported in the literature, although KNiO$_2$ is scarcely reported. According to Kim *et al.,* density functional theory calculations indicate that KNiO$_2$ is not thermodynamically stable.[136] ***Figure 6****a* shows that smaller metal ions such as Ni cannot accommodate a sufficiently large distance between K$^+$ ions, resulting in non-layered pyramidal structures rather than layered prismatic or octahedral structures. Alternatively, ***Figure 6****b* reveals that KScO$_2$ and KCrO$_2$ are the most

stable K-based layered oxide structures according to density functional theory calculations. By exploring a different avenue of research, honeycomb-structured $K_{0.66}Ni_{0.66}Te_{0.33}O_2$ is reported by Masese and colleagues as a cathode material with considerably higher average voltage than standard K^+ layered oxide cathodes, as shown in *Figure 6*.[137] In a K^+ half-cell, the $K_{0.66}Ni_{0.66}Te_{0.33}O_2$ cathode delivers 70.0 mAh g^{-1} of the 128 mAh g^{-1} theoretical capacity. Honeycomb structured tellurates may present attractive framework materials for further doping as Masese *et al.* demonstrate that Mg and Co can also be incorporated into the structure.[137]
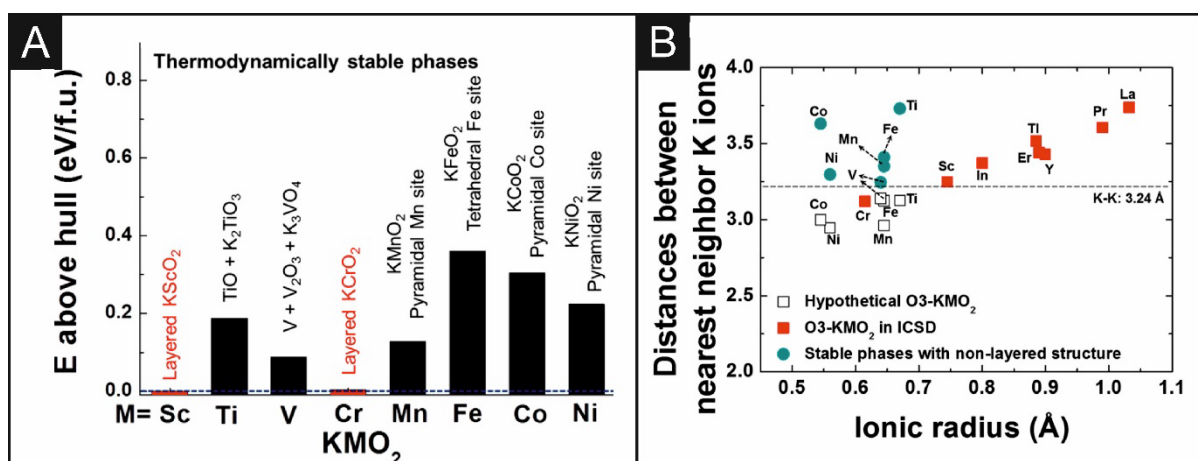
Figure 6. A) The K^+-K^+ distance within the layered structure in relation to the ionic radius of the transition metal used. The white squares reveal hypothetically unstable structures, and the orange squares indicate stable layered structures as reported in the ICSD, and the green circles represent stable non-layered structures. B) the thermodynamically stable phases of layered K compounds.[136]

4. Binary metal oxides

4.1. $ACo_xMn_yO_2$ where A = Li, Na, K

4.1.1. $LiCo_xMn_yO_2$

Early literature by Myung *et al.* states that partially substituting the Mn component in $LiMnO_2$ by more than 5% causes a phase transition to distorted monoclinic, which has a detrimental effect on the reversible capacity.[138] Furthermore, substituting the relative large Mn^{3+} ions of $LiMnO_2$ with smaller Co^{3+} ions is likely to decrease the interplanar spacing and thus hinder the ion transport kinetics. Shaju *et al.* investigate a lithiated $O2-Li_{0.66}Co_{0.15}Mn_{0.85}O_2$ to reveal an initial discharge capacity of 143 mAh g^{-1} for the non-lithiated sample and 210 mAh g^{-1} for the lithiated sample.[42] Although 62.0 mAh g^{-1} of this is lost in the first cycle. Few reports exist for this cathode material, possibly due to the irreversibility of Li^+ extraction and the need for extensive pre-lithiation strategies.[43]

4.1.2. $NaCo_xMn_yO_2$

Layered oxides containing both Co and Mn benefit from increased thermal stability and enhanced rate capability.[139] The P2-type phases are more commonly used over the O3 types due to their enhanced structural stability. However, the P2-types are susceptible to capacity decay due to the P2-O2 phase transition at ~4.2 V.[140] This often limits the operating voltage range of these cathode materials. The theoretical capacity of $Na_{1.0}Co_{0.7}Mn_{0.3}O_2$ at maximum Na^+ extraction is 237.6 mAh g^{-1}, 210 mAh g^{-1} of which can be achieved experimentally at a high voltage of 4.5 V.[141] However, this capacity is not maintained through subsequent cycles due to the irreversibility of Na^+ extraction at higher voltages. At a lower cut off voltage of 4.1 V, capacity retention of 84.0 % over 225 cycles is achieved at 1 C. At a slightly increased cut off voltage of 4.15 V, high capacity retention of 99.0% at a charge rate of 5 C over 100 cycles is achieved. Likewise, $P2-Na_{0.67}Co_{0.5}Mn_{0.5}O_2$ displays impressive cycling performance with a capacity retention of close to 100% over 100 cycles at a current rate of 1 C in the range of 1.5-4.3 V, attributed to the host structure's flexibility.[140] 88.0 mAh g^{-1} of capacity is retained after 2000 cycles at an increased current rate of 30 C, capacity retention of 47.0 %. In contrast, Wang *et al.* also synthesised $P2-Na_{0.66}Mn_{0.5}Co_{0.5}O_2$ and found it to have capacity retention of 69.0 % over 30 cycles at 30.0 mAh g^{-1}.[142] They compared this to $P2-Mn_{0.66}CoO_2$ and $P2-Mn_{0.66}MnO_2$

to conclude that increasing the Mn content increases the initial charge capacity but has a detrimental effect on the cycling stability.

Li *et al.* report that low-spin Co^{3+} and Ni^{2+} ions increase the Na^+ diffusion coefficient as the ion diffusion channels are enlarged.[143] This contributes to an improved rate capability compared to $Na_{0.7}Mn_{0.7}Ni_{0.3}O_2$. To reduce structural distortions and further enhance the rate capability, Wang *et al.* vary the Co content of $Na_{0.66}Co_xMn_{0.66-x}Ti_{0.34}O_2$ from 0-0.33, with 0.22 to provide a capacity of 120 mAh g^{-1} at 1 C.[144] Ti-doping reduces structural distortions, whilst the increase of Co^{3+} encourages a higher average valance state of $Mn^{3.7+}$ to minimise Jahn-Teller distortions arising from Mn^{3+}. Furthermore, Mo-doping is used to increase the capacity retention of $Na_{0.59}Co_{0.20}Mn_{0.80}O_2$, which in turn also increases the reversible capacity to 131.9 mAh g^{-1} at 0.1 C, 91.5% of which is retained over 100 cycles.[145] This is due to three main advantages: Mo-doping enhances the stability of the crystal structure by shortening the metal-oxygen bond, decreasing the cation disorder and facilitating higher bond energy between Mo-O compared to the Co and Mn equivalents. In comparison, Zr-doping results in a higher reversible capacity of 172 mAh g^{-1} at 0.1 C but suffers more capacity decay during cycling, with a capacity retention of 88.0% after 50 cycles for $Na_{0.7}Mn_{0.8}Co_{0.15}Zr_{0.05}O_2$.[146] In broader applications, P2-type layered $Na_{0.5}Co_{0.5}Mn_{0.5}O_2$ has also shown potential within room temperature seawater batteries, acting as an oxygen electrocatalyst to achieve a discharge capacity of 183 mAh g^{-1} within a hard carbon full cell.[147]

4.1.3. $KCo_xMn_yO_2$

A P3-$K_{0.45}Mn_{0.5}Co_{0.5}O_2$ cathode achieves a capacity of 140 mAh g^{-1}, higher than that of P2-$K_{0.6}CoO_2$ and P3-$K_{0.45}MnO_2$ with capacities of 71.0 and 128 mAh g^{-1}, respectively. [27, 92, 148] Furthermore, the high rate capability at 100 mA g^{-1} is maintained at 68 mAh g^{-1}, which is a slight increase from 65.0 mAh g^{-1} compared to $K_{0.6}CoO_2$.[92] Choi *et al.* demonstrated using X-ray absorption near-edge structure (XANES) analysis to reveal that the Co^{3+} substitutes Mn^{3+} encouraging an average oxidation state of Mn^{4+}.[149] This inhibits the Jahn-Teller distortions from Mn^{3+}, resulting in smooth charge-discharge profiles compared to K_xMnO_2 materials. The P2- and P3-type phases are the most stable structures for the materials mentioned above, but they suffer from K-deficiencies, limiting the amount of K^+ that can be reversibly extracted before the structural collapse.[149] Resultantly, future research efforts should reveal dopants, coatings or additives that increase the K-content.

4.2. $AMn_xNi_yO_2$

4.2.1. $LiMn_xNi_yO_2$

Changing the morphology has a significant influence on electrochemical performance. The variations of Li-rich LiMnNiO2 cathodes tend to suffer from severe capacity decay and insufficient rate capability due to electrolyte decomposition and poor conductivity of surface layers formed during cycling.[43] In terms of performance, LiMnxNiyO2 cathodes are proposed as an alternative to LiCoO2, with higher rate performance. He *et al.* synthesised a nanoscale $Li_{1.2}Mn_{0.6}Ni_{0.2}O_2$ material that achieves a superior capacity of 221 mAh g^{-1} at a charge rate of 20.0 mA g^{-1} and an impressive 118 mAh g^{-1} at a high charge rate of 1000 mA g^{-1}.[150] A nano-/micro spherical $Li_{1.2}Ni_{0.2}Mn_{0.6}O_2$ cathode achieves a notably high capacity of 299 mAh g^{-1}, alongside capacity retention of 81.0 % at 0.1 C and up to 94.4% at 0.5 C over 200 cycles.[46] Additionally, 3D reticular $Li_{1.2}Ni_{0.2}Mn_{0.6}O_2$ microparticles of 2 μm size and a mesoporous nanostructure were synthesised by Li *et al.*, delivering a capacity of 196 mAh g^{-1} and 136 mAh g^{-1} at 10 C and 1000 mA g^{-1}, respectively.[44] A high capacity of 95.6% over 50 cycles at 1 C is observed.

Mn-based layered cathodes are prone to voltage fade, which is often mitigated by post-fabrication coating with Li$^+$ conductive materials.[98, 99] Furthermore, improvements in capacity are typically achieved with transition metal element doping.[151, 152] As seen in earlier sections, a Li_2ZrO_3 coating improves the electrochemical performance of a LiCoO2 cathode.[52] In order to yield the benefits of both Li_2ZrO_3 coating and Zr^{4+} doping, Zhang *et al.* use a synchronous lithiation method, whereby the Li_2ZrO_3 coating and the $Li_{1.2}Mn_{0.6}Ni_{0.2}O_2$ layers are formed simultaneously by reaction with LiOH.[153] ***Figure 7***a highlights the difference in a synchronous lithiation and post-coating method and the effect on the crystalline phase. ***Figure 7***b shows that the rate performance of $Li_{1.2}Mn_{0.6}Ni_{0.2}O_2$ is improved further by synchronous lithiation of $Li_{1.2}Mn_{0.6}Ni_{0.2}O_2$ than the post-coated $Li_{1.2}Mn_{0.6}Ni_{0.2}O_2$. The synchronous lithiation Li_2ZrO_3 coating improves the capacity from 139 mAh g^{-1} to 168 mAh g^{-1} at 1 C when cycled between 2.5-4.8 V, as displayed in ***Figure 7***c. Furthermore, the capacity retention of 70.1% for the bare electrode is improved to 77.6% and 83.5% for the post-coated $Li_{1.2}Mn_{0.6}Ni_{0.2}O_2$ and synchronous lithiation $Li_{1.2}Mn_{0.6}Ni_{0.2}O_2$, respectively. Due to the stabilising effect of the increased proportion of Zr^{4+} from the synchronous lithiation $Li_{1.2}Mn_{0.6}Ni_{0.2}O_2$, the average operational voltage is 0.15 V higher than the uncoated sample, as shown in ***Figure 7***c. The synchronous lithiation method combines the benefits of Li_2ZrO_3 coating with Zr^{4+} doping to

25

increase the Li^+ conductivity of the electrode surface, thus resulting in overall enhanced electrochemical performance compared to both the uncoated and post-coated $Li_{1.2}Mn_{0.6}Ni_{0.2}O_2$ electrode.
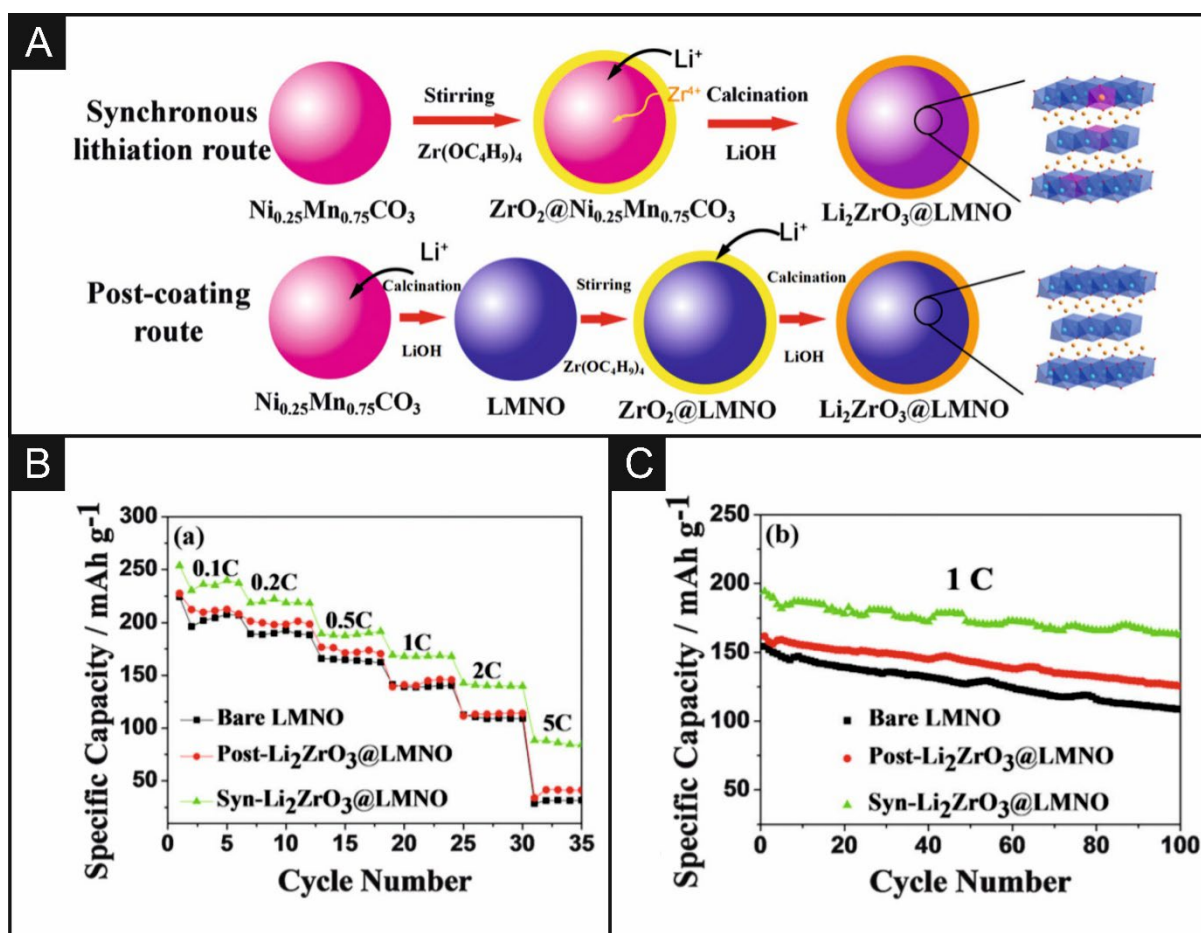
Figure 7. *A) Schematic of $Li_{1.2}Mn_{0.6}Ni_{0.2}O_2/Li_2ZrO_3$ synthesised via synchronous lithiation and a post-coating route. Electrochemical performance of $Li_{1.2}Mn_{0.6}Ni_{0.2}O_2/Li_2ZrO_3$ in terms of B) rate performance and C) specific capacity.[153]*

Li *et al.* reveal that Coulombic efficiency is often limited due to the evolution of oxygen from the electrode surface and thus proposes a Ba dopant to stabilise oxygen radicals during charging.[154] Although this results in comparatively lower capacity and cycling stability. Carroll *et al.* suggest that the oxygen loss at the surface is due to the reduction of Mn at the surface.[155] The resulting vacant oxygen sites contribute to electrolyte decomposition and thus leading to the formation of a segregated spinel-phase surface layer. Liu *et al.* propose co-modifying the $Li_{1.2}Ni_{0.2}Mn_{0.6}O_2$ surface with NH_4F and Al_2O_3 to increase the Coulombic efficiency without compromising the capacity.[156] The Coulombic efficiency increases from 82.7% to 87.5% upon modification, alongside a capacity increase from 253 mAh g^{-1} to 287 mAh g^{-1} at C/20. This is attributed to minor oxygen evolution from the electrode surface and stabilisation of the Ni redox couple. Zang *et al.* partially substituted Mn^{4+} with Mo^{6+} to form $Li_{1.2}Ni_{0.2}Mn_{0.59}Mo_{0.01}O_2$, which exhibited a capacity of 245 mAh g^{-1} at 0.1 C, 93.2% of which is retained over 204 cycles[45].

$Li_{1.2}Mn_{0.6}Ni_{0.2}O_2$ exhibits capacity retention of 187 mAh g^{-1}, marginally higher than $Li_{1.2}Mn_{0.55}Ni_{0.2}O_2$ at 171 mAh g^{-1} at 0.5 C.[157] Although, the lower Mn content in $Li_{1.2}Mn_{0.55}Ni_{0.2}O_2$ facilitates higher capacity retention of 88.7% over 100 cycles and a significantly lower voltage decay per cycle. Significantly reduced amount of layered material transferred into the spinel phase, which is the proposed reason for the lower capacity and voltage decay. However, Feng *et al.* found spinel $LiNi_{0.5}Mn_{1.5}O_4$ to retain 95.0 % of its 125 mAh g^{-1} capacity over 200 cycles at 1 C, in addition to Gao *et al.* that found the same spinel cathode to exhibit capacity retention of 97.0 % over 100 cycles at 0.1 C and 96.1% at 5 C.[158, 159] Excellent capacity retentions upwards of 97% over 100 cycles at 0.5 C are achieved with spinal-type $LiNi_{0.5}Mn_{1.5}O_4$ *via* RuO_2 coating or doping.[160-162] Further advances in capacity, capacity retention and average voltage are achieved with surface coatings such as ZrO_2,[163] conductive carbon,[164, 165] La_2O_3,[166] and dopants such as Nb,[167, 168] Al,[169-171] and Mg[172] to name a few. Spinal-type $LiNi_{0.5}Mn_{1.5}O_4$ is a separate research direction that could lead to fruitful research advances in electrochemical performance.[173]

4.2.2. $NaMn_xNi_yO_2$

P2-NaMnNiO₂ has a high theoretical capacity of 172 mAh g^{-1}.[174] Although they are susceptible to irreversible phase transitions to O2-type structures, which result in lower capacities and poor stability.[175, 176] With a wide voltage range of 1.5 -4.5 V, a P2-$Na_{0.66}Ni_{0.33}Mn_{0.66}O_2$ cathode

28

delivers an initial discharge capacity of 228 mAh g^{-1} without the use of bulk dopants or surface coating.[174] However, the capacity retention is inferior at 40.0 % after 100 cycles at 0.05 C. Limiting the voltage range to 2.0-4.0 results in a vastly improved capacity retention of 96.0 % over 100 cycles but considerably reduces the capacity to 89.0 mAh g^{-1}. Similarly, low capacities of 68.0 -89.0 mAh g^{-1} are reported in the 2.0-4.0 V range by other groups.[177, 178]

Demonstrating the influence of structural morphology and synthesis route, P2-type $Na_{0.66}Ni_{0.33}Mn_{0.66}O_2$ micro flakes synthesised *via* a co-precipitation method yield a capacity of 152 mAh g^{-1}, with 81.0 % of this initial capacity retained after 50 cycles.[179] The structural changes during charging are fully reversible, with no O2-type phases observed. Furthermore, with a P2-$Na_{0.66}Ni_{0.33}Mn_{0.66}O_2$ nanowire cathode, the capacity retention of 81.0% can be extended over 500 cycles, with an initial capacity of 167 mAh g^{-1}.[180] P2-type $Na_{0.66}Ni_{0.33}Mn_{0.66}O_2$ plates synthesised *via* a spray pyrolysis method results in a superior rate performance, with a capacity retentions of 93.0 -99.0 % over 200 cycles at 0.1 C, dependent on particle size.[177] However, the capacities of 69.0 -86.0 mAh g^{-1} are much lower than other $Na_{0.66}Ni_{0.33}Mn_{0.66}O_2$ examples.

Although the P2 phases are renowned for higher structural stability, the O3 phases generally have higher initial capacity.[25] Chen *et al.* documents a hybrid O3/P2 phase $Na_{0.88}Ni_{0.45}Mn_{0.55}O_2$ cathode that delivers a reversible capacity of 107 mAh g^{-1}, with a reversible capacity of 71.0% at 1 C over 250 cycles.[181] The low stability of the O3 is confirmed as O3-$Na_{0.9}Ni_{0.45}Mn_{0.55}O_2$ delivers a higher capacity of 124 mAh g^{-1} but capacity retention of only 38.3%. Furthermore, at a higher charge rate of 10 C, the hybrid O3/P2 cathode maintains 72.4% of the initial discharge capacity over 1000 cycles. Partial substitution of the Mn and Ni components with other transition metals such as F[182, 183], B[182], Sn, Mg[184], Mo[185, 186], Co[175], Zn[187, 188] and Cu[176, 189] are commonplace throughout literature as a method of avoiding phase transitions and thus increasing stability. Wang *et al.* investigate the use of non-metallic elements in improving the performance of a P3-$Na_{0.65}Mn_{0.75}Ni_{0.25}O_2$ cathode.[182] It is demonstrated that doping with F mitigates irreversible phase transitions into the O2 phase and B doping causes a phase transition from the P3 phase into the P2 phase, thus increasing the stability of the layered structure. Furthermore, Chen *et al.* also reported the influence of F in improving the cycling stability,

producing a $Na_{0.6}Mn_{0.95}Ni_{0.05}O_{1.95}F_{0.05}$ cathode that retains 75% of its capacity over 960 cycles at 2 C.[183]

Wang *et al.* report a $Na_{0.67}Ni_{0.1}Cu_{0.2}Mn_{0.7}O_2$ cathode that delivers a reversible capacity of 125 mAh g^{-1}, 17% lower than that of pristine $Na_{0.67}Ni_{0.3}Mn_{0.7}O_2$.[176] This is because a proportion of the Ni ions are replaced by larger Cu ions, which lowers the theoretical capacity and reduces the amount of Na$^+$ that can be reversibly extracted. However, after 40 cycles, the Cu-doped cathodes show higher capacity than the pristine sample, owing to the suppression of the P2-O2 phase transition. In contrast, Liu *et al.* report a P2-$Na_{0.44}Mn_{0.6}Ni_{0.4}O_2$ cathode that can be Cu-doped without compromising the capacity.[189] The capacity retention is improved with Cu-doping from 59.5% to 80.9% over 50 cycles at 0.1 C. This may be because the Ni content in $Na_{0.44}Mn_{0.6}Ni_{0.3}Cu_{0.1}O_2$ is higher than that of $Na_{0.67}Ni_{0.1}Cu_{0.2}Mn_{0.7}O_2$ reported by Wang *et al.*[176] Alternatively, Hou *et al.* use Co-doping to avoid the presence with the O2 phase, thus achieving capacity retention of 73.8% over 100 cycles at 0.1 C with a capacity that has slightly improved from 160 mAh g^{-1} to 164 mAh g^{-1}.[175] Moreover, incorporation of Mo^{6+} into the crystal structure has a stabilising effect.[185] Notably high capacity retention of 86% over 1200 cycles at a high charge rate of 10 C and 89.6% over 100 cycles at 0.1 C.[186]

4.2.3. KMn$_x$Ni$_y$O$_2$

As mentioned in the context of Li$^+$ and Na$^+$ batteries, Mn-based layered oxides are promising cathodes due to their high theoretical capacities and straightforward, low-cost synthesis.[139] However, they are also susceptible to Jahn-Teller distortions arising from the presence of Mn^{3+}. Consequently, Ni is incorporated into the structure of binary KMnO$_2$ oxides. Bai *et al.* demonstrate that P3-$K_{0.67}Mn_{0.83}Ni_{0.17}O_2$ achieves an initial discharge capacity of 122 mAh g^{-1} at 0.2 C, alongside capacity retention of 75.0% at 5 C for 200 cycles.[190] This is a slight improvement on the 115 mAh g^{-1} capacity of the $K_{0.67}MnO_2$ cathode used as a benchmark, but a significant improvement compared to the P3-type $K_{0.5}MnO_2$ demonstrated by Kim *et al.* that delivers 81.0 mAh g^{-1}.[117] It also exceeds the estimated theoretical capacity of 111 mAh g^{-1}.[191] In comparison, a $K_{0.67}Mn_{0.92}Ni_{0.08}O_2$ cathode retains only 48.0% of its capacity, whilst the $K_{0.67}Mn_{0.67}Ni_{0.33}O_2$ cathode retains 68.0%. Thus, balancing the Mn and Ni-content of the $K_{0.67}Mn_{0.83}Ni_{0.17}O_2$ electrode sufficiently stabilises the layered structure to endure the volume expansions during extraction and insertion of K.[190] P2-type $K_{0.44}Ni_{0.22}Mn_{0.78}O_2$ synthesised by Zhang *et al.* achieves a higher capacity of 126 mAh g^{-1} at 10 mA g^{-1} with a capacity retention

of 80.0% over 30 cycles.[192] Additionally, capacity retention of 90.0% over 500 cycles is observed in a soft carbon full cell. When the half-cell is cycled at 10 mA g^{-1} to 500 mA g^{-1} and back to 20.0 mA g^{-1}, 112 mAh g^{-1} of the original 126 mAh g^{-1} capacity is recovered, the cathode can endure the structural expansion during insertion and extraction of relatively large K ions. Jo *et al.* demonstrated that a P2-$K_{0.75}Ni_{0.33}Mn_{0.66}O_2$ cathode delivers 110 mAh g^{-1} at a current rate of 20.0 mA g^{-1} with a capacity retention of 86.0% over 300 cycles.[191] At a high rate of 1400 mA g^{-1}, the material still exhibits a capacity of 91.0 mAh g^{-1}, 83.0% of which is retained over 500 cycles. Stabilising the material against the P2-O2 phase transition avoids the capacity decay due to excessive volume expansion, as seen in P2-$Na_{0.66}Ni_{0.33}Mn_{0.66}O_2$.[193] The enhanced electrochemical performance is ascribed to the Ni^{4+}/Ni^{2+} redox couple.

In comparison, incorporating Fe to form $K_{0.75}Mn_{0.8}Ni_{0.1}Fe_{0.1}O_2$ results in a capacity of 100 mAh g^{-1} at 1 C in a voltage range of 1.5-3.9 V.[194] At both 1 C and 10 C, the capacity retention is 70.0% over 200 cycles. Choi *et al.* utilised a distorted P2 phase to achieve a high capacity of 155 mAh g^{-1} at 52.0 mA g^{-1}.[96] The voltage range extends to an upper cut off voltage of 4.3 V, similar to Jo *et al.*,[191] but higher than 3.8 V used by Bai *et al.*[190] and 4.0 V used by Zhang *et al.*[192] Extending the upper cut off voltage generally results in higher capacity, but often results in more significant capacity decay. However, in the voltage range of 1.5-4.3 V, the P'2-$K_{0.83}Ni_{0.05}Mn_{0.95}O_2$ cathode retains 77.0 % of the 155 mAh g^{-1} is retained over 500 cycles. There is room for improvement in ensuring higher cycling stability whilst ensuring a wide voltage window.

5. Ternary metal oxides and beyond

5.1. $ANi_xMn_yCo_zO_2$

5.1.1. $LiNi_xMn_yCo_zO_2$

Although advantageous from a cost and environmental perspective, completely removing Co negatively affects the ion diffusion kinetics, resulting in lower rate capabilities.[195] However, layered materials with the general formula $LiNi_xCo_yMn_zO_2$ (where x + y + z = 1) have significantly less Co content than $LiCoO_2$ cathodes whilst providing similar or higher capacity. The doping of Li-NMC materials to form quaternary layered oxides further reduces the required amount of Co. Zhang *et al.* reported that $Li_{1.2}Ni_{0.13}Co_{0.13}Mn_{0.54}O_2$ delivers a capacity of 226 mAh g^{-1} at 200 mA g^{-1}, 79% of which is retained over 500 cycles.[152] At a lower charge rate of 0.2 C, 95% of the 285 mAh g^{-1} capacity is retained over 50 cycles. The superior cycling stability is attributed to the use of a Na-CMC binder. Although the Na-CMC binder enhances

stability, compared to a PVDF binder, it causes a reduction in capacity and efficiency. Furthermore, $LiNi_{0.8}Co_{0.1}Mn_{0.1}O_2$ achieves a lower capacity of 146.6 mAh g^{-1} but has a high capacity retention of 94.7% over 100 cycles at a charge rate of 1 C.[196] In addition, Pham *et al.* reveals that a functional polyimide binder permits an increase in upper cut-off voltage from 4.2 to 4.4 V.[197]

Yoo *et al.* report that a $LiNi_{0.6}Co_{0.2}Mn_{0.2}O_2$ retains 90.8% of its 206 mAh g^{-1} over 30 cycles at 0.05C, which is marginally improved to 206 mAh g^{-1} and a 94.5% capacity retention when a nano-Al_2O_3 coating is applied by improving the ionic conductivity and Li$^+$ intercalation.[198] When compared to the example above, Al_2O_3 coated $LiNi_{0.6}Co_{0.2}Mn_{0.2}O_2$ achieves a higher capacity of 166 mAh g^{-1} at 1 C. Furthermore, a Li_2ZrO_3 coating on a $LiNi_{0.7}Co_{0.15}Mn_{.15}O_2$ cathode results in a graphite full-cell pouch battery that achieves impressive capacity retention of 73.3% over 1500 cycles at a charge rate of C/3.[199] In a half cell, Li_2ZrO_3 coating exhibits a high discharge capacity of 190 mAh g^{-1}, 85.0% of which is retained over 50 cycles at 0.1 C.[76] The beneficial effect of Li_2ZrO_3 coating is further confirmed by Xu *et al.* with a coated $LiNi_{0.5}Co_{0.2}Mn_{0.3}O_2$ cathode that delivers 194 mAh g^{-1} at 0.2 C.[77] Similarly, Wang *et al.* and Liang *et al.* achieve similar capacity retentions with a Li_2ZrO_3 coating.[200, 201] Furthermore, utilising ZrO_2, the capacity retention of 75.6% over 100 cycles for $LiNi_{0.6}Co_{0.2}Mn_{0.2}O_2$ is improved to 83.8% in the voltage range of 2.8-4.3 V at 0.1 C upon the incorporation of ZrO_2 nanoparticles (*circa* 50nm).[202] Yao *et al.* demonstrates that a ZrO_2 surface coating on a $LiNi_{0.6}Co_{0.2}Mn_{0.2}O_2$ cathode can retain good capacity retention of 82.5% in the higher voltage range of 2.8-4.5 V.[203] To ensure a homogenous surface coating, Ho *et al.* propose the use of thioacetamide as a support for the ZrO_2 coatings, which would act as an interface adhesive layer promoting the distribution and adhesion to the substrate surface.[204]

A SiO_2 coated $LiNi_{0.8}Co_{0.1}Mn_{0.1}O_2$ cathode delivers a capacity of 201 mAh g^{-1}, with a capacity retention of 87.3% over 100 cycles at 0.5 C, which reduces only slightly to 84.5% over 100 cycles at 55°C.[205] Cho *et al.* confirm that SiO_2 coating enhances the thermal stability and suppresses side reactions[206], alongside Khollari *et al.,* who utilised a reduced graphene oxide combined SiO_2 coating[207], illustrated by *Figure 8*a, and Zhao *et al.* who used a 3D-SiO_2 framework.[208] The FESEM images and elemental distribution in *Figure 8*b and c show that the reduced graphene oxide forms an evenly distributed layer over the SiO_2 coating. The capacity

retention of 80.0% over 100 cycles and discharge capacity of 187 mAh g^{-1} is attributed to the synergistic effect of SiO$_2$ protecting against side reactions and the reduced graphene oxide layer enhancing the ion diffusion kinetics and conductivity.[207, 209] The SEM images in *Figure 8* shows that the particle size and morphology remain the same upon SiO$_2$ coating. However, the 3.0 wt% SiO$_2$ coating appears to show agglomeration.[206, 210] Dai *et al.* reported that a CaF$_2$ coating improves the capacity retention of LiNi$_{0.8}$Co$_{0.1}$Mn$_{0.1}$O$_2$ cycled at 55°C from 59.0% over 50 cycles at 1 C, to 79.7%, whilst the capacity remains constant at ~150 mAh g^{-1}.[211] To avoid unwanted side reactions that can result in loss of capacity, Zhu *et al.* employed a Nd$_2$O$_3$ layer to segregate the LiNi$_{0.8}$Co$_{0.1}$Mn$_{0.1}$O$_2$ material from the electrolyte.[212] This increased the capacity retention from 78.7% to 88.0% over 100 cycles at 1 C. Furthermore, at an elevated temperature of 55°C, the capacity of the pristine sample increased from 158 mAh g^{-1} to 171 mAh g^{-1}, accompanied by improved capacity retention over 50 cycles from 78.9% to 85.5%.
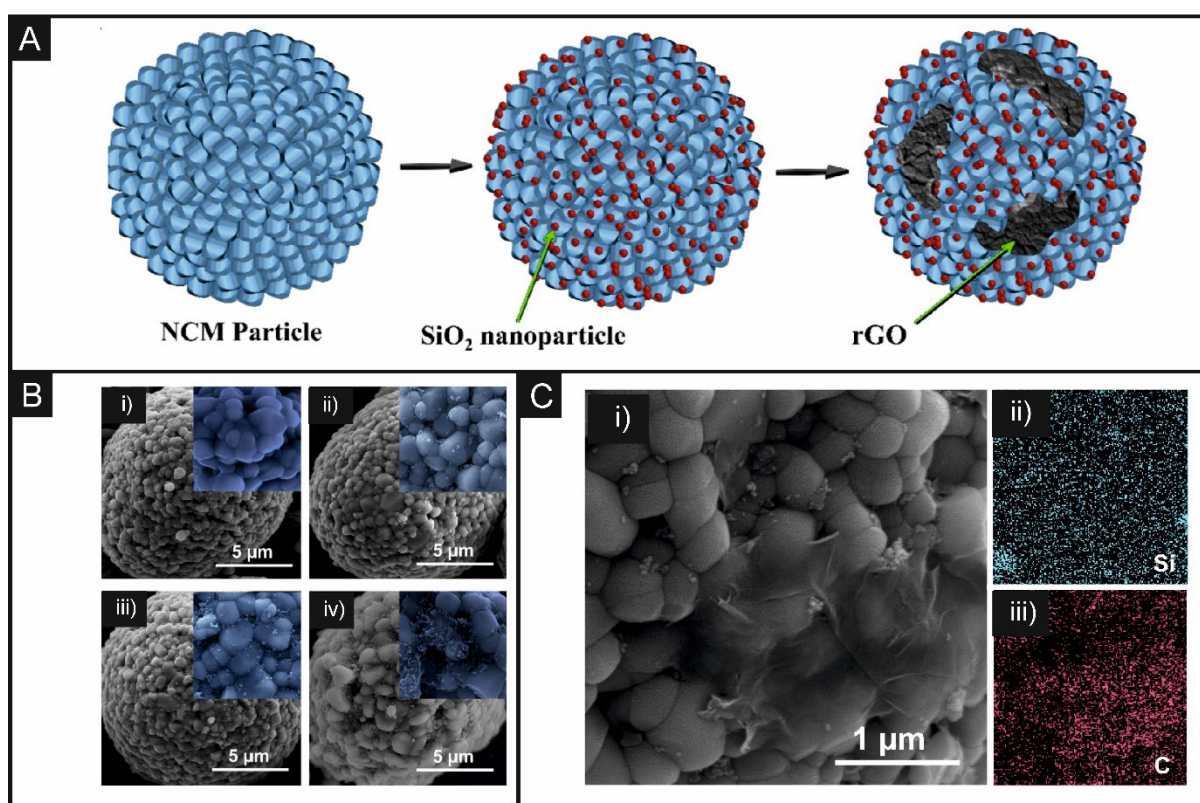
Figure 8. *A) Schematic synthesis of reduced graphene oxide-SiO$_2$ coated LiNi$_{0.5}$Co$_{0.2}$Mn$_{0.3}$O$_2$ B) FESEM image of (i) pristine NCM, (ii) 0.5, (iii) 1 and (iv) 3 wt% SiO$_2$-NCM cathode material. The insets show a magnified image.[207] C) i) FESEM image of reduced graphene oxide-SiO$_2$ coated LiNi$_{0.5}$Co$_{0.2}$Mn$_{0.3}$O$_2$ cathode and elemental distribution of ii) Si and iii) C.[206]*

Ti is used in surface coatings such as $Li_4Ti_5O_{12}$ to improve ion diffusion and inhibit side reactions, resulting in an increase in capacity retention from 39.4% of the pristine electrode to 75.9% for the coated electrode at 1 C in the range of 2.7-4.3 V.[213] Although, $Li_4Ti_5O_{12}$ is more commonly utilised as a negative electrode material[214-216] alongside dopants such as F,[217, 218] Ru,[219] and Y[220], to name a few. Remaining on the theme of Ti-based coatings, the capacity retention is improved from 78.1% to 88.7% at 1 C between 3.0-4.5 V by using a TiO_2 coated $LiNi_{0.6}Co_{0.2}Mn_{0.2}O_2$ cathode.[221] Tian *et al.* revealed that reconstruction of the surface to the rock salt structure leads to low coulombic efficiencies in the first cycle, which is reduced by Ti doping.[195] Therefore, Yao *et al.* co-doped a $LiNi_{0.8}Co_{0.1}Mn_{0.1}O_2$ cathode with K and Ti to fabricate a graphite full-cell that achieves a first charge efficiency of 84.0%.[55] K and Ti co-doping also improves the overall electrochemical performance as a high capacity of 173.4 mAh g^{-1} was recorded, 91.6% of which is retained over 200 cycles at a charge rate of 0.2 C. In terms of capacity, Zhang *et al.* reported a capacity of 215 mAh g^{-1} for $LiNi_{0.8}Co_{0.1}Mn_{0.1}Ti_{0.005}O_2$ at a charge rate of 0.1 C between 2.8-4.3 V.[222] Whereas Du *et al.* uses 2% Ti-doped $LiNi_{0.8}Co_{0.1}Mn_{0.1}O_2$ to extend the voltage range to 2.8-4.5 V, whilst still achieving a capacity of 206 mAh g^{-1} at 0.1 C.[223] Ti-doping is beneficial as it enhances structural stability by increasing the strength of the Ni-O bonds.[224] Na-doping holds many environmental and cost advantages over other elements as it is highly abundant at a low cost. When used as a dopant for $LiNi_{0.6}Co_{0.2}Mn_{0.2}O_2$, Na^+ improves the capacity retention from 83.7% at 1 C over 100 cycles to 93.5%.[225] The capacity at 0.1 was 178 mAh g^{-1} and 184 mAh g^{-1} for an un-doped and a doped sample respectively.

Nb-doping is also used throughout literature as it minimises capacity loss arising from charge transfer resistance, resulting in a quaternary $Li_{1.2}Ni_{0.13}Co_{0.13}Mn_{0.54}O_2$ Nb cathode with a capacity of 281.3 mAh g^{-1} with a capacity retention of 88.0% over 100 cycles.[151] Furthermore, Lei *et al.* used Nb-doping to facilitate an increase of the upper cut-off voltage to 4.6 V, resulting in a 10.7% increase in capacity retention.[226]

At a low charge rate of 0.5 C, the capacity retention of a Mo-doped $LiNi_{0.5}Co_{0.2}Mn_{0.3}O_2$ was 152 mAh g^{-1}, with a capacity retention of 97.1% over 50 cycles.[227] Even at a higher charge rate of 8 C, a capacity of 125 mAh g^{-1} is achieved. It should be noted that the voltage range used throughout is limited at 3.0-4.3 V. In contrast, Ta-doping allows for a capacity of 148 mAh g^{-1} with a capacity retention of 83.5% over 100 cycles at 1 C with a higher cut-off voltage of 3.0-

4.5 V.[228] Y-doping by 4 mol % delivers a discharge capacity of 207 mAh g^{-1} for LiNi$_{0.8}$Co$_{0.1}$Mn$_{0.1}$O$_2$ as well as increasing the first cycle efficiency from 79.2% to 81.4% in a relatively high voltage range of 2.8-4.5 V.[229] Although, the capacity of the modified sample is lower than that of the uncoated sample as the LiYO$_2$ coating is electrochemically inactive, it simply acts as a Li$^+$ conductive layer. The capacity retention of a 2 mol % Y-doped cathode is notably high at 98.4% of the 189 mAh g^{-1} capacity being retained over 100 cycles at 0.5 C. In comparison to coating, which achieves a charge capacity of 189 mAh g^{-1} at 0.1 C and 149 mAh g^{-1} at 1 C.[229] Although this does not improve the capacity compared to the bare sample, it increases the capacity retention from 85.1% to 91.5% over 100 cycles at 1 C. Xu *et al.* also reports capacity retention using Y$_2$O$_3$ from 78.6% to 87.8% over 50 cycles for a LiNi$_{0.5}$Co$_{0.2}$Mn$_{0.3}$O$_2$ cathode.[230] Chen *et al.* continued using Y$_2$O$_3$ coating to achieve an electrode with a notably high capacity of 280 mAh g^{-1} at 0.5 C, 89.1% of which is retained over 200 cycles.[231]

Li-NMC cathodes perform comparatively well when considering the balance between capacity retention and capacity, summarised in *Figure 9*. In a graphite full cell, 1.0 mol% W-doping of LiNi$_{0.9}$Co$_{0.05}$Mn$_{0.05}$O$_2$ increases the capacity retention from 60.0% over 500 cycles at 1 C, to 89.0%.[232] The capacity remains constant at ~235 mAh g^{-1}. Zhang *et al.* report a lower capacity of 204 mAh g^{-1} for W-doped LiNi$_{0.8}$Mn$_{0.1}$Co$_{0.1}$O$_2$, good capacity retention of 92.1% over 100 cycles at 1 C is achieved.[233] Under an equivalent charge rate of 1 C, a WO$_3$ coating a LiNi$_{0.8}$Co$_{0.1}$Mn$_{0.1}$O$_2$ cathode increases the capacity retention by 16.7% from 58.5% over 100 cycles to 68.3%.[234] However, at a charge rate of 0.2 C, 82.1% of the 182 mAh g^{-1} capacity is retained over 100 cycles for the WO$_3$ coated cathode. Mg can be incorporated into the structure of LiNi$_{0.8}$Co$_{0.12}$Mn$_{0.05}$O$_2$ by co-precipitation of (Ni$_{0.83}$Co$_{0.12}$Mn$_{0.05}$)$_{1-x}$Mg$_x$(OH)$_2$ (x = 0.25-0.30) and Ni$_{0.83}$Co$_{0.12}$Mn$_{0.05}$(OH)$_2$ with LiOH to avoid severe structural degradation for at least 200 cycles.[235] Mg-doping improves the capacity retention from 74% to 87.2%, with a high reversible capacity of 199.7 mAh g^{-1}. Huang *et al.* also used Mg-doping with a co-precipitation method, confirming that Mg-doping increases capacity retention. An increase from 79.3% to 90.0% over 100 cycles at 1 C.[236] In a full-cell, Li$_{0.97}$Ni$_{0.8}$Co$_{0.1}$Mn$_{0.1}$Mg$_{0.03}$O$_2$ shows a high energy density of 595 W h kg^{-1}, alongside a capacity of 183 mAh g^{-1} at 0.1 C.[237]
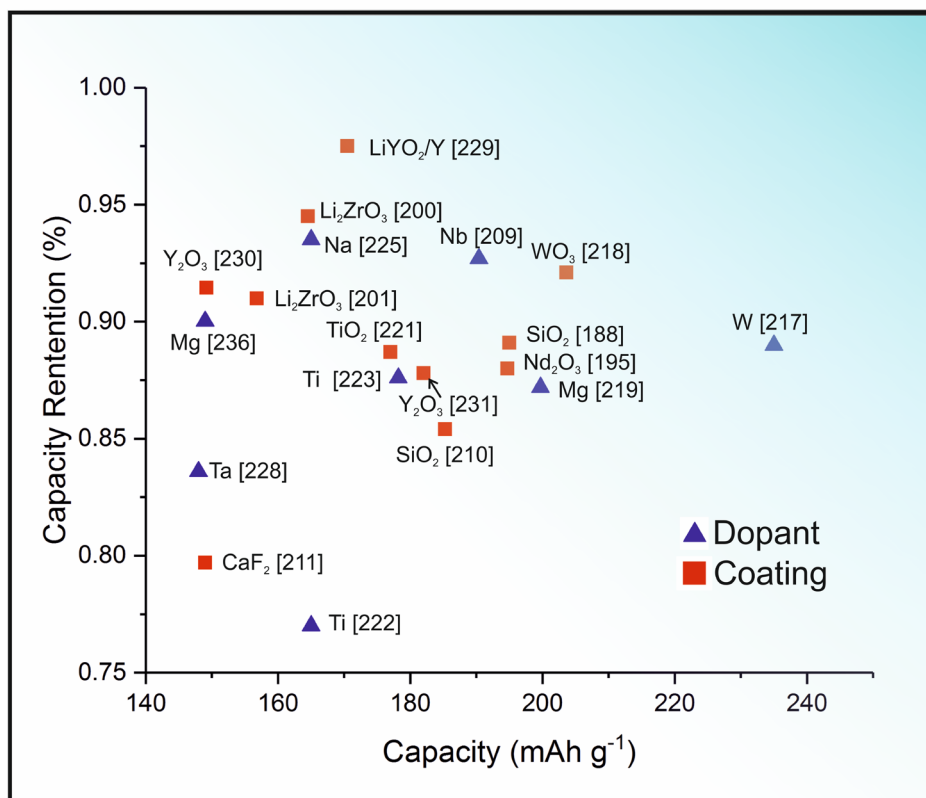
Figure 9. *Summary of key results reported in the literature shows the extent of the inconsistency in reports, testing procedures and results throughout the field.*

5.1.2. $NaNi_xMn_yCo_zO_2$

Single and binary layered oxides have been studied at length towards Na^+ batteries, revealing the need to incorporate additional transition metals to mitigate the poor rate performance, especially at higher charge rates. Consequently, $NaNi_xMn_yCo_zO_2$ materials have emerged as cathode materials with higher structural stability, thus overcoming the rate capability issues. The electrochemistry is influenced by particle size and distribution, with micro- and nanoparticles having shorter diffusion pathways and thus enhanced transfer kinetics. This can be achieved using sol-gel,[143, 238, 239] Pechini,[240] and a mix of co-precipitation and solid-state synthesis methods.[241-244] A $Na_{0.65}Ni_{0.17}Co_{0.11}Mn_{0.72}O_2$ cathode synthesised *via* solid-state reaction yields an initial discharge capacity of 190 mAh g^{-1} at 12.0 mA g^{-1} with a low capacity retention of 55.0 % over 100 cycles between 1.5-4.3 V.[241] In contrast, $Na_{0.65}Ni_{0.17}Co_{0.11}Mn_{0.72}O_2$ with microspherical morphology *via* a co-precipitations method shows much-improved capacity retention of 91.0 %, whilst the capacity remains relatively constant at 187 mAh g^{-1}.[241] Also achieved by a co-precipitation method, O3-$NaNi_{0.6}Co_{0.2}Mn_{0.2}O_2$ and P2-$Na_{0.7}Ni_{0.6}Co_{0.2}Mn_{0.2}O_2$ achieved discharge capacities of 153 mAh g^{-1} and 145 mAh g^{-1}, respectively between 2.0-4.0 V at 0.1 C.[243] When the upper cut off voltage is increased to 4.3 V, the P2- achieves a higher discharge capacity of 175 mAh g^{-1}. In terms of stability, the P2-type material retains 96.0 % of its capacity over 100, compared to a capacity retention of 52.0 % for the O3 type.

Furthermore, an initial discharge capacity of 141 mAh g^{-1} and capacity retention of 89.0 % over 50 cycles is achieved by a $Na_{0.67}Mn_{0.65}Co_{0.2}Ni_{0.15}O_2$ micro flake cathode from a sol-gel synthesis method.[238] The capacity retention can be improved to 95.4% over 50 cycles upon Al-substitution to form $Na_{0.67}Mn_{0.65}Ni_{0.15}Co_{0.15}Al_{0.05}O_2$. Additionally, Rangasamy *et al.* increase the capacity by using acetate-based sol-gel precursors over the traditional nitrate based.[239] The platelet-like morphology of the $NaMn_{0.33}Ni_{0.33}Co_{0.33}O_2$ derived from acetate-based precursors leads to a higher surface area, leading to lower charge-transfer resistance.

In contrast, P2-$Na_{0.66}Mn_{0.54}Ni_{0.13}Co_{0.13}O_2$ cathodes fabricated using a modified Pichini method can endure a wide voltage range of 2.0-4.5 V with a 148 mAh g^{-1} capacity at a charge rate of 160 mA g^{-1}.[240] However, the capacity retention remains an area for future improvements. Bao *et al.* report that a higher Na^+ content significantly improves the cycling stability, with $Na_{0.67}Ni_{0.167}Co_{0.167}Mn_{0.167}O_2$ showing optimal performance with an initial discharge capacity of 123 mAh g^{-1}, 95.0% of which is retained over 50 cycles.[245] Although the lower Na^+ content of $Na_{0.45}Ni_{0.167}Co_{0.167}Mn_{0.167}O_2$ results in a higher initial discharge capacity of 143 mAh g^{-1}, it

suffers severe capacity decay in the following cycles. A Na^+ content of below 0.55 causes a proportion of the layered structure to form the P3-phase, whereas Na^+ content of 0.67 or above allows for the retention of crystalline P2-phase, even after 200 cycles. Na^+ content of 0.80 and above tends to result in large particle sizes, which is detrimental to the ion diffusion kinetics. Sathiya *et al.* reported a $Na_{0.33}Mn_{0.33}Co_{0.33}O_2$ cathode that achieves a capacity of 120 mAh g^{-1}, despite the low Na^+ content, but this is achieved in the limited voltage range of 2.0-3.75 V.[246] After exposure to air for 15 and 30 days, the growth of Na_2CO_3 can be observed on the particle surfaces. Confirmed by XRD and IR analysis, NaOH and Na_2CO_3 during the cycling of $Na_{0.33}Mn_{0.33}Co_{0.33}O_2$ arise from an O3 to O1, then P3 phase transition, indicating that the material is unstable against H_2O and CO_2 exposure.[246] The materials are often limited to low cut off voltages to balance the need for high capacity and high capacity retention. Hwang *et al.* utilised an Al_2O_3 surface coating to increase the capacity retention of $NaNi_{0.6}Co_{0.2}Mn_{0.2}O_2$ from 80.0% over 50 cycles at 0.1 C to 91.0%, with a low cut off voltage of 4.1 V.[247] Additionally, an Al_2O_3 coated $Na_{0.66}Mn_{0.54}Ni_{0.13}Co_{0.13}O_2$ cathode fabricated by atomic layer deposition achieves a capacity of 123 mAh g^{-1} in a more extensive voltage range of 2.0-4.5 V but exhibits poor capacity retention. The capacity retention can be improved by employing a lower cut off voltage of 4.3 V, but subsequently lowers the capacity to 81.0 mAh g^{-1}.[240] In an attempt to mitigate this, Bao *et al.* engineered a $Na_{0.67}Ni_{0.167}Co_{0.167}Mn_{0.67}O_2$ electrode with a Ni-rich bulk and an Mn-rich surface, forming a transition metal concentration gradient.[244] The enhanced ion diffusion kinetics facilitated by the smaller particles on the surface results in capacity retention of 87.0 % over 100 cycles, improved from 55.0 %. However, the voltage peak is still observed at 4.5 V, indicative of the irreversible P2-O2 phase transition. Good capacities and excellent capacity retentions are obtained with $NaCo_xMn_yNi_zO_2$, and future research efforts should aim to improve performance at higher cut off voltages, thus allowing for further capacity increases. Many of the coatings and dopants listed for the Li^+ counterparts could be investigated for their usefulness towards Na^+ battery cathodes.

5.1.3. $KNi_xCo_yMn_zO_2$

As K^+ ions are larger than their Li^+ and Na^+ counterparts, cathodes that have yielded success within Li^+ and Na^+ batteries may not transfer to K^+ batteries. Binary layered oxides such as P3-$K_{0.67}Mn_{0.83}Ni_{0.17}O_2$ and P3-$K_{0.45}Mn_{0.5}Co_{0.5}O_2$ have shown reasonably high capacities over 122 mAh g^{-1} but require improvements in terms of rate capability and capacity retention.[148, 190] Ternary layered oxides are lesser studied towards K^+ batteries. Materials such as P3-type

$K_{0.5}Mn_{0.8}Fe_{0.1}Ni_{0.1}O_2$ have been reported but still suffer from limited capacity retentions and low upper cut-off voltages.[248] A $K_{0.67}Ni_{0.17}Co_{0.17}Mn_{0.66}O_2$ cathode with an average voltage of 3.1 V is reported by Liu *et al.*[249] The cathode achieves a capacity of 76.5 mAh g^{-1}, 87.0% of which is retained over 100 cycles at 0.2 C. The Coulombic efficiency of 97.6% and the reversibility of K extraction is good, and the electrode shows good capacity recovery. Deng et al. synthesised a P3-type $K_{0.5}Mn_{0.72}Ni_{0.15}Co_{0.13}O_2$ microsphere cathode that can achieve a high energy density per volume and enhanced ion diffusion to improve the rate capability kinetics due to the smaller particle sizes.[250] The rate capability is 57.9 mAh g^{-1} at 500 mA g$^{-1,}$ and 85.0% of the capacity is retained over 100cycls 50.0 mA g^{-1}, which drops to 75.0% over 300 cycles at 200 mA g^{-1}. Although lowering the current rate to 10 mA g^{-1} allows for a higher capacity of 82.5 mAh g^{-1}, it causes a decline in capacity retention.

To mitigate the slow ion diffusion kinetics and synchronously increase the rate capability, Xu *et al.* engineered a microspherical and microcubic combined morphology P3 type $K_{0.48}Ni_{0.2}Co_{0.2}Mn_{0.6}O_2$ cathode.[251] ***Figure 10***a-c shows that the cathode has an even distribution of the cubic and spherical microparticles, which in turn have a homogenous distribution of each transition metal within (***Figure 10***e-f). Furthermore, the XPS spectra in ***Figure 10***g show Ni, Co and Mn in the expected valance states indicative of a layered structure. After 150 cycles, at around 0.5 C, capacity retention of 76.2% is achieved. However, the first discharge capacity is limited to 57.0 mAh g^{-1} at around 0.5 C and 35.0 mAh g^{-1} at around 4 C. This value can be increased using a higher cut-off voltage, although at the expense of stability. Dang *et al.* investigated the influence of Mg and Al doping on a $K_{0.45}Ni_{0.1}Co_{0.1}Mn_{0.8}O_2$ cathode. A pristine $K_{0.45}Ni_{0.1}Co_{0.1}Mn_{0.8}O_2$ cathode shows a poor charge capacity of 34.3 mAh g^{-1} with a low capacity retention of 38.5% over 100 cycles at 20.0 mA g^{-1}.[252] The Al- and Mg-doped electrodes improve the capacity retention to 77.4% and 74.3%, respectively, with the Al-doped electrode facilitating the highest discharge capacity of 65.0 mAh g^{-1}. However, the first discharge capacity of 89.2 mAh g^{-1} for the pristine electrode is reduced to 80.8 mAh g^{-1} and 84.5 mAh g^{-1} for the Mg- and Al-doped electrodes, respectively, likely due to the lower Mn^{3+} content. In terms of rate capability, the Al-doped $K_{0.45}Ni_{0.1}Co_{0.1}Al_{0.05}Mn_{0.75}O_2$ electrode shows a reversible capacity of 79.0 mAh g^{-1} at 10.0 mA g^{-1}, dropping to 37.0 mAh g^{-1} at a high rate of 500 mA g^{-1}, compared to 14 mAh g^{-1} for the pristine sample. When the current rate is lowered back to 10.0 mA g^{-1}, the electrode shows good capacity recovery as 72.0 mAh g^{-1} is achieved. Na-doping increases the capacity of the pristine P3-$K_{0.67}Ni_{0.17}Co_{0.17}Mn_{0.66}O_2$ from 76.1 mAh

g^{-1} to 86.1 mAh g^{-1} at 20.0 mA g^{-1}, 97.1% and 91.5% of which is retained over 10 and 100 cycles, respectively.[253] At a higher current rate of 100 mA g^{-1}, 62.0 mAh g^{-1} is still achieved. There is progress ahead in achieving a reasonable rate capability over an extended voltage range without compromising capacity retention. The effects of dopants and surface coatings have not been exhaustively explored, which provides an avenue for future research.
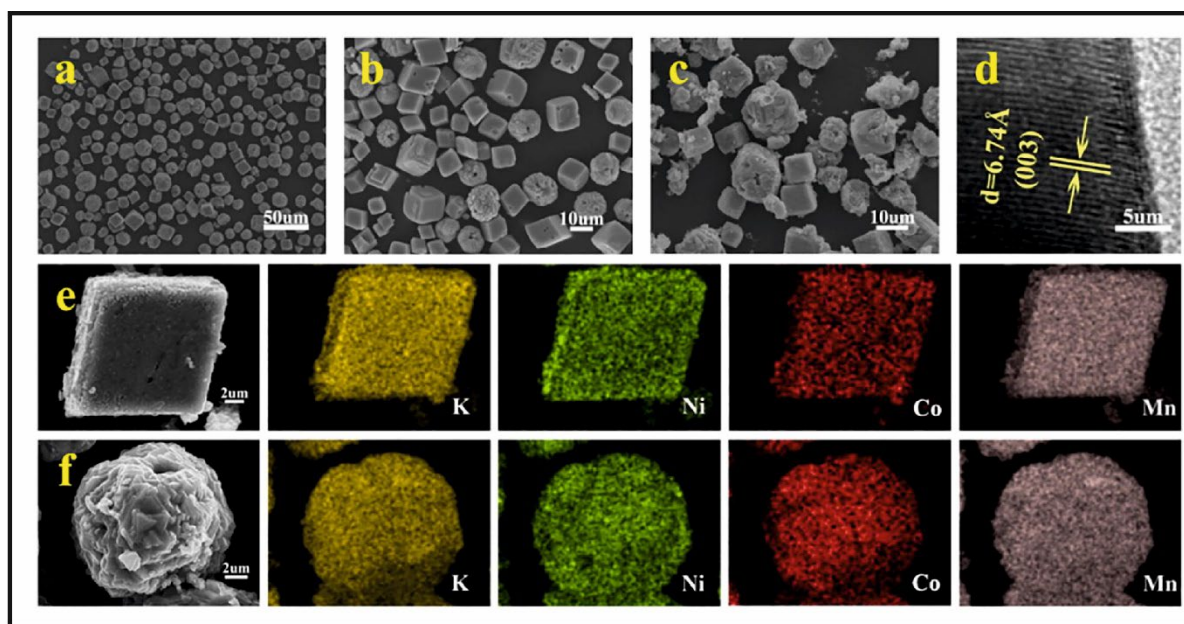
Figure 10. *A) The mixed morphologies of P3 type $K_{0.48}Ni_{0.2}Co_{0.2}Mn_{0.6}O_2$, showing a-c) the presence of microsphere and microcubic morphologies within the bulk material. d) TEM image of $K_{0.48}Ni_{0.2}Co_{0.2}Mn_{0.6}O_2$. The elemental distribution of K, Ni, Co and Mn within e) microcubes and f) microspheres.*

6. Conclusions

This review has overviewd the extensive work directed to $ACo_xMn_yNi_zO_2$ and metal oxides as cathode materials for metal-ion batteries which is to not to entirely replace Li^+ batteries but to partially alleviate the demand by offering more sustainable alternatives to operate as large-scale energy storage systems. A current limitation for Li^+, Ni^+ and K^+ batteries is their limited capabilities at high voltages and irreversible phase changes often occur at high cut off voltages around 4.5 V, resulting in fast capacity decay which reduce the voltage range often increases the stability, but in turn, reduces the capacity. New research is starting to be directed to stabilising the layered oxide crystal structure against detrimental phase changes at high voltages and elevated temperatures would lead to a next-generation class of versatile and high voltage batteries and future work should continue this endeavour.

Although Li^+ batteries and their compositions, coatings and dopants continue to be extensively explored, they must be assessed in terms of their practicality towards industrial-scale usage in large-scale energy storage systems. Although elements such as Nb,[226] Y[229] and Ta[228] improve the electrochemical performance of a Li^+ cathode, their low abundance and relatively high cost render them unlikely candidates for use in commercial energy storage systems.[254] Furthermore, concerns of the toxicity, availability and price of Ni and Co has instigated efforts to replace these with elements such as Fe and Cu.[255, 256] With sustainability in mind, modern research is beginning to establish methods of reclaiming and recycling lithium from spent batteries.[257] Compatible anodes must be revealed for potential metal-ion battery cathodes. Whereas a graphite anode serves Li^+ batteries, these are not widely used in Na^+ and K^+, leaving considerations between hard carbon,[258] disordered carbon,[259] Ti-based[259, 260] as popular anodes for non-Li^+ systems. Non-electrode factors such as SEI layer formation and its implications towards Na^+ and K^+ batteries are not yet fully understood, providing aTHis n area for improving electrochemical performance.[258, 261, 262] Moreover, efforts to replace organic solvent electrolytes due to their potential safety hazards are ongoing, revealing non-flammable alternatives such as ionic liquids[263] and polymer-based[264, 265] electrolytes.

43

Conflict of Interest

The authors declare no conflict of interest

References

1. T. Kim, W. Song, D.-Y. Son, L. K. Ono and Y. Qi, *Journal of Materials Chemistry A*, 2019, **7**, 2942-2964.
2. C. Zhao, Y. Lu, L. Chen and Y.-S. Hu, *Nano Research*, 2019, **12**.
3. Y. Wang, R. Chen, T. Chen, H. Lv, G. Zhu, L. Ma, C. Wang, Z. Jin and J. Liu, *Energy Storage Mater.*, 2016, **4**, 103-129.
4. W. Liu and D. B. Agusdinata, *J. Clean Prod.*, 2020, **260**, 120838.
5. D. B. Agusdinata, W. Liu, H. Eakin and H. Romero, *Environ. Res. Lett.*, 2018, **13**, 123001.
6. K. Chayambuka, G. Mulder, D. L. Danilov and P. H. L. Notten, *Advanced Energy Materials*, 2018, **8**, 1800079.
7. C. Delmas, *Advanced Energy Materials*, 2018, **8**, 9.
8. Y. Fang, L. Xiao, Z. Chen, X. Ai, Y. Cao and H. Yang, *Electrochemical Energy Reviews*, 2018, **1**, 294-323.
9. L. Chen, M. Fiore, J. E. Wang, R. Ruffo, D.-K. Kim and G. Longoni, *Advanced Sustainable Systems*, 2018, **2**, 1700153.
10. Y. C. Liu, B. Huang, Y. J. Shao, M. Y. Shen, L. Du and S. J. Liao, *Prog. Chem.*, 2019, **31**, 1329-1340.
11. R. Rajagopalan, Y. Tang, X. Ji, C. Jia and H. Wang, *Adv. Funct. Mater.*, 2020, **30**, 35.
12. C. Vaalma, D. Buchholz and S. Passerini, *Current Opinion in Electrochemistry*, 2018, **9**, 41-48.
13. Z. Shadike, E. Zhao, Y.-N. Zhou, X. Yu, Y. Yang, E. Hu, S. Bak, L. Gu and X.-Q. Yang, *Advanced Energy Materials*, 2018, **8**, 1702588.
14. K. Matsumoto, J. Hwang, S. Kaushik, C.-Y. Chen and R. Hagiwara, *Energy & Environmental Science*, 2019, **12**, 3247-3287.
15. A. Eftekhari, Z. Jian and X. Ji, *ACS Appl. Mater. Interfaces*, 2017, **9**, 4404-4419.
16. G. Steinhauser, *J. Clean Prod.*, 2008, **16**, 833-841.
17. C. Vaalma, G. A. Giffin, D. Buchholz and S. Passerini, *J. Electrochem. Soc.*, 2016, **163**, A1295-A1299.
18. Y. Li, Y. Lu, C. Zhao, Y.-S. Hu, M.-M. Titirici, H. Li, X. Huang and L. Chen, *Energy Storage Mater.*, 2017, **7**, 130-151.
19. A. W. Golubkov, D. Fuchs, J. Wagner, H. Wiltsche, C. Stangl, G. Fauler, G. Voitic, A. Thaler and V. Hacker, *RSC Advances*, 2014, **4**, 3633-3642.
20. X. Zhu, T. Mochiku, H. Fujii, K. Tang, Y. Hu, Z. Huang, B. Luo, K. Ozawa and L. Wang, *Nano Research*, 2018, **11**, 6197-6205.
21. B. L. Ellis, W. R. M. Makahnouk, Y. Makimura, K. Toghill and L. F. Nazar, *Nature materials*, 2007, **6**, 749-753.
22. A. K. Padhi, K. S. Nanjundaswamy and J. B. Goodenough, *J. Electrochem. Soc.*, 1997, **144**, 1188-1194.
23. J. J. Wang and X. L. Sun, *Energy & Environmental Science*, 2015, **8**, 1110-1138.
24. I. Sultana, M. M. Rahman, S. Mateti, N. Sharma, S. M. Huang and Y. Chen, *Batteries Supercaps*, 2020, **3**, 450-455.
25. M. H. Han, E. Gonzalo, G. Singh and T. Rojo, *Energy & Environmental Science*, 2015, **8**, 81-102.
26. S. Mariyappan, Q. Wang and J. M. Tarascon, *J. Electrochem. Soc.*, 2018, **165**, A3714-A3722.
27. C.-l. Liu, S.-h. Luo, H.-b. Huang, Y.-c. Zhai and Z.-w. Wang, *Chem. Eng. J.*, 2019, **356**, 53-59.
28. Y. Zhang, N. Xiaogang, L. Tan, L. Deng, S. Jin, L. Zeng, H. Xu and Y. Zhu, *ACS Applied Materials & Interfaces*, 2020, **XXXX**.
29. Y. Xu, X. Deng, Q. Li, G. Zhang, F. Xiong, S. Tan, Q. Wei, J. Lu, J. Li, Q. An and L. Mai, *Chem*, 2019, **5**, 1194-1209.
30. P. Wang, X. Shi, Z. Wu, S. Guo, J. Zhou and S. Liang, *Carbon Energy*, 2020, **n/a**.
31. D. Kundu, B. D. Adams, V. Duffort, S. H. Vajargah and L. F. Nazar, *Nature Energy*, 2016, **1**, 16119.

45

32. M. E. Arroyo-de Dompablo, A. Ponrouch, P. Johansson and M. R. Palacín, *Chem. Rev.*, 2019.
33. K. Zhang, D. Kim, Z. Hu, M. Park, G. Noh, Y. Yang, J. Zhang, V. W. Lau, S. L. Chou, M. Cho, S. Y. Choi and Y. M. Kang, *Nat Commun*, 2019, **10**, 5203.
34. M. Arroyo-de Dompablo, C. Krich, J. Nava-Avendaño, M. Palacín and F. Barde, *Phys. Chem. Chem. Phys.*, 2016, **18**.
35. E. Gonzalo, M. H. Han, J. M. López del Amo, B. Acebedo, M. Casas-Cabanas and T. Rojo, *J. Mater. Chem. A*, 2014, **2**, 18523-18530.
36. E. Lee, J. Lu, Y. Ren, X. Luo, X. Zhang, J. Wen, D. Miller, A. DeWahl, S. Hackney, B. Key, D. Kim, M. D. Slater and C. S. Johnson, *Advanced Energy Materials*, 2014, **4**, 1400458.
37. K. Mizushima, P. C. Jones, P. J. Wiseman and J. B. Goodenough, *Mater. Res. Bull.*, 1980, **15**, 783-789.
38. K. V. Kravchyk, P. Bhauriyal, L. Piveteau, C. P. Guntlin, B. Pathak and M. V. Kovalenko, *Nat Commun*, 2018, **9**, 4469.
39. X. Li, Z. Su and Y. Wang, *J. Alloys Compd.*, 2018, **735**, 2182-2189.
40. W. Tong, Q. Chu, Y. Meng, X. Wang, Y. Bin, J. Gao, X. Zhao and X. Liu, *Materials Research Express*, 2018, **5**, 065511.
41. M. Tian, Y. Gao, Z. Wang and L. Chen, *PCCP*, 2016, **18**, 17345-17350.
42. K. M. Shaju, G. V. Subba Rao and B. V. R. Chowdari, *Solid State Ionics*, 2002, **152-153**, 69-81.
43. K. M. Shaju, K. V. Ramanujachary, S. E. Lofland, G. V. Subba Rao and B. V. R. Chowdari, *J. Mater. Chem.*, 2003, **13**, 2633-2640.
44. L. Li, L. Wang, X. Zhang, Q. Xue, L. Wei, F. Wu and R. Chen, *ACS Appl. Mater. Interfaces*, 2017, **9**, 1516-1523.
45. Y. Zang, C.-X. Ding, X.-C. Wang, Z.-Y. Wen and C.-H. Chen, *Electrochim. Acta*, 2015, **168**, 234-239.
46. Y. Li, Y. Bai, X. Bi, J. Qian, L. Ma, J. Tian, C. Wu, F. Wu, J. Lu and K. Amine, *ChemSusChem*, 2016, **9**, 728-735.
47. N. Yabuuchi and T. Ohzuku, *J. Power Sources*, 2003, **119-121**, 171-174.
48. J. Choi and A. Manthiram, *Journal of The Electrochemical Society - J ELECTROCHEM SOC*, 2005, **152**.
49. Y. Miao, P. Hynan, A. von Jouanne and A. Yokochi, *Energies*, 2019, **12**, 1074-1094.
50. S. Kalluri, M. Yoon, M. Jo, S. Park, S. Myeong, J. Kim, S. X. Dou, Z. Guo and J. Cho, *Advanced Energy Materials*, 2017, **7**, 1601507.
51. S. Sheng, G. Chen, B. Hu, R. Yang and Y. Xu, *J. Electroanal. Chem.*, 2017, **795**, 59-67.
52. J. Zhang, R. Gao, L. Sun, H. Zhang, Z. Hu and X. Liu, *Electrochim. Acta*, 2016, **209**, 102-110.
53. L.-W. Jiang, Y.-X. Lu, Y. Wang, L.-L. Liu, X. Qi, C.-L. Zhao, L.-Q. Chen and Y.-S. Hu, *Chin. Phys. Lett.*, 2018, **35**, 048801.
54. D. Sehrawat, J. Zhang, D. Yu and N. Sharma, *Small Methods*, 2018, 1800092.
55. W. Yao, Y. Liu, D. Li, Q. Zhang, S. Zhong, H. Cheng and Z. Yan, *The Journal of Physical Chemistry C*, 2020, **124**, 2346-2356.
56. L. Xu, F. Zhou, B. Liu, H. Zhou, Q. Zhang, J. Kong and Q. Wang, *International Journal of Electrochemistry*, 2018, **2018**, 6930386.
57. B. R. Babu, P. Periasamy, R. Thirunakaran, N. Kalaiselvi, T. P. Kumar, N. G. Renganathan, M. Raghavan and N. Muniyandi, *International Journal of Inorganic Materials*, 2001, **3**, 401-407.
58. B. Ammundsen, J. DeSilvestro, T. Groutso, D. Hassell, J. B. Metson, E. Regan, R. Steiner and P. J. Pickering, San Francisco, Ca, 1999.
59. M. S. Whittingham, J. D. Guo, R. J. Chen, T. Chirayil, G. Janauer and P. Zavalij, *Solid State Ionics*, 1995, **75**, 257-268.
60. J. Chen, S. Wang and M. S. Whittingham, *Journal of Power Sources*, 2007, **174**, 442-448.
61. C. Julien and S. S. Michael, *Ionics*, 1998, **4**, 181-190.
62. T. H. Cho, S. M. Park, M. Yoshio, T. Hirai and Y. Hideshima, *Journal of Power Sources*, 2005, **142**, 306-312.

46

63.   H. Liu, Y. P. Wu, E. Rahm, R. Holze and H. Q. Wu, *Journal of Solid State Electrochemistry*, 2004, **8**, 450-466.

64.   C. Julien, L. El-Farh, S. Rangan and S. Massot, *Journal of Sol-Gel Science and Technology*, 1999, **15**, 63-72.

65.   M. A. Khan, D. Han, G. Lee, Y.-I. Kim and Y.-M. Kang, *J. Alloys Compd.*, 2019, **771**, 987-993.

66.   V. Etacheri, 2017, pp. 155-195.

67.   J. Lamb and A. Manthiram, *Chemistry of Materials*, 2020, **32**, 8431-8441.

68.   S. J. Shi, J. P. Tu, Y. Y. Tang, Y. X. Yu, Y. Q. Zhang and X. L. Wang, *Journal of Power Sources*, 2013, **221**, 300-307.

69.   S. J. Shi, S. S. Zhang, Z. J. Wu, T. Wang, J. B. Zong, M. X. Zhao and G. Yang, *Journal of Power Sources*, 2017, **337**, 82-91.

70.   D. W. Su, C. Y. Wang, H. J. Ahn and G. X. Wang, *Chemistry-a European Journal*, 2013, **19**, 10884-10889.

71.   Y. B. Shen, H. J. Xue, S. H. Wang, D. Y. Zhang, D. M. Yin, L. M. Wang and Y. Cheng, *Chemical Engineering Journal*, 2021, **411**, 10.

72.   J. B. Goodenough, *Prog. Solid State Chem.*, 1971, **5**, 145-399.

73.   J.-N. Zhang, Q. Li, C. Ouyang, X. Yu, M. Ge, X. Huang, E. Hu, C. Ma, S. Li, R. Xiao, W. Yang, Y. Chu, Y. Liu, H. Yu, X.-Q. Yang, X. Huang, L. Chen and H. Li, *Nature Energy*, 2019, **4**, 594-603.

74.   J. B. Goodenough and H. Gao, *Science China Chemistry*, 2019, **62**, 1555-1556.

75.   R. Fathi, J. Burns, D. Stevens, H. Ye, C. Hu, E. Scott, C. Schmidt and J. Dahn, *J. Electrochem. Soc.*, 2014, **161**, A1572-A1579.

76.   S. Sun, C. Du, D. Qu, X. Zhang and Z. Tang, *Ionics*, 2015, **21**.

77.   Y. Xu, Y. Liu, Z. Lu, H. Wang, D. Sun and G. Yang, *Appl. Surf. Sci.*, 2016, **361**, 150-156.

78.   A. Zhou, J. Xu, X. Dai, B. Yang, Y. Lu, L. Wang, C. Fan and J. Li, *J. Power Sources*, 2016, **322**, 10-16.

79.   H. Liu, C. Chen, C. Du, X. He, G. Yin, B. Song, P. Zuo, X. Cheng, Y. Ma and Y. Gao, *Journal of Materials Chemistry A*, 2015, **3**, 2634-2641.

80.   A. Zhou, W. Wang, Q. Liu, Y. Wang, X. Yao, F. Qing, E. Li, T. Yang, L. Zhang and J. Li, *J. Power Sources*, 2017, **362**, 131-139.

81.   N. Ohta, K. Takada, I. Sakaguchi, L. Zhang, R. Ma, K. Fukuda, M. Osada and T. Sasaki, *Electrochem. Commun.*, 2007, **9**, 1486-1490.

82.   G. Li, S. Zhou, P. Wang and J. Zhao, *RSC Advances*, 2015, **5**, 107326-107332.

83.   S.-T. Myung, N. Kumagai, S. Komaba and H.-T. Chung, *Solid State Ionics*, 2001, **139**, 47-56.

84.   M. C. Rao and O. M. Hussain, *J. Alloys Compd.*, 2010, **491**, 503-506.

85.   K. Sivajee Ganesh, B. Purusottam reddy, P. Jeevan Kumar and O. M. Hussain, *J. Electroanal. Chem.*, 2018, **828**, 71-79.

86.   B. Hu, X. Lou, C. Li, F. Geng, C. Zhao, J. Wang, M. Shen and B. Hu, *J. Power Sources*, 2019, **438**, 226954.

87.   H. Xia, Y. Wan, W. Assenmacher, W. Mader, G. Yuan and L. Lu, *NPG Asia Materials*, 2014, **6**, e126-e126.

88.   L. Gao, S. Chen, H. Hu, H. Cheng, L. Zhang and X. Yang, *Mater. Lett.*, 2020, **260**, 126965.

89.   Y. Fang, X. Y. Yu and X. W. D. Lou, *Angew. Chem. Int. Ed. Engl.*, 2017, **56**, 5801-5805.

90.   S. Hwang, Y. Lee, E. Jo, K. Y. Chung, W. Choi, S. M. Kim and W. Chang, *ACS Appl. Mater. Interfaces*, 2017, **9**, 18883-18888.

91.   H. Kim, J. C. Kim, S.-H. Bo, T. Shi, D.-H. Kwon and G. Ceder, *Advanced Energy Materials*, 2017, **7**, 1700098.

92.   T. Deng, X. Fan, C. Luo, J. Chen, L. Chen, S. Hou, N. Eidson, X. Zhou and C. Wang, *Nano Lett.*, 2018, **18**, 1522-1529.

93.   K. Sada, B. Senthilkumar and P. Barpanda, *Chem. Commun.*, 2017, **53**, 8588-8591.

94.   Y. Hironaka, K. Kubota and S. Komaba, *Chem. Commun.*, 2017, **53**, 3693-3696.

47

95. Y.-S. Xu, S.-Y. Duan, Y.-G. Sun, D.-S. Bin, X.-S. Tao, D. Zhang, Y. Liu, A.-M. Cao and L.-J. Wan, *Journal of Materials Chemistry A*, 2019, **7**, 4334-4352.

96. J. U. Choi, Y. Ji Park, J. H. Jo, Y. H. Jung, D.-C. Ahn, T.-Y. Jeon, K.-S. Lee, H. Kim, S. Lee, J. Kim and S.-T. Myung, *Energy Storage Mater.*, 2020, **27**, 342-351.

97. H. Zhao, J. Wang, G. Wang, S. Liu, M. Tan, X. Liu and S. Komarneni, *Ceram. Int.*, 2017, **43**, 10585-10589.

98. J. Cho, T.-J. Kim and B. Park, *Journal of The Electrochemical Society - J ELECTROCHEM SOC*, 2002, **149**.

99. A. Nagasubramanian, D. Y. W. Yu, H. Hoster and M. Srinivasan, *J. Solid State Electrochem.*, 2014, **18**, 1915-1922.

100. C. Chang, J. Dong, L. Guan and D. Zhang, *Materials (Basel, Switzerland)*, 2019, **12**, 468.

101. D. Luo, S. Fang, L. Yang and S.-i. Hirano, *Journal of Materials Chemistry A*, 2016, **4**, 5184-5190.

102. L. Zhang, *International Journal of Electrochemical Science*, 2019, **14**, 2422-2429.

103. J. Billaud, R. J. Clément, A. R. Armstrong, J. Canales-Vázquez, P. Rozier, C. P. Grey and P. G. Bruce, *J. Am. Chem. Soc.*, 2014, **136**, 17243-17248.

104. T. Ma, G.-L. Xu, X. Zeng, Y. Li, Y. Ren, C. Sun, S. M. Heald, J. Jorne, K. Amine and Z. Chen, *J. Power Sources*, 2017, **341**, 114-121.

105. V. Dall'Asta, D. Buchholz, L. Chagas, X. Dou, C. Ferrara, E. Quartarone, C. Tealdi and S. Passerini, *ACS Applied Materials & Interfaces*, 2017, **9**.

106. M. Xu, Y. Niu, C. Chen, J. Song, S. Bao and C. M. Li, *RSC Advances*, 2014, **4**, 38140-38143.

107. Y. Zhang, Y. Ouyang, L. Liu, J. Xia, S. Nie, W. Liu and X.-y. Wang, *Journal of Central South University*, 2019, **26**, 1510-1520.

108. G. Ma, Y. Zhao, K. Huang, Z. Ju, C. Liu, Y. Hou and Z. Xing, *Electrochim. Acta*, 2016, **222**.

109. D. Zhang, W.-j. Shi, Y.-w. Yan, S.-d. Xu, L. Chen, X.-m. Wang and S.-b. Liu, *Electrochim. Acta*, 2017, **258**.

110. Y. Liu, X. Liu, F. Bu, X. Zhao, L. Wang, Q. Shen, J. Zhang, N. Zhang, L. Jiao and L.-Z. Fan, *Electrochim. Acta*, 2019, **313**.

111. C. Ferrara, C. Tealdi, V. Dall'Asta, D. Buchholz, L. Chagas, E. Quartarone, V. Berbenni and S. Passerini, *Batteries*, 2018, **4**, 8.

112. D. Wang, Y. Liu, Z. Wu, X. Liu, J. Qu, H. Liu, Y. Ming, Y. Zhong, B. Zhong and X. Guo, *Chem. Commun.*, 2020, **56**, 2921-2924.

113. W.-J. Shi, Y.-W. Yan, C. Chi, X.-T. Ma, D. Zhang, S.-D. Xu, L. Chen, X.-M. Wang and S.-B. Liu, *J. Power Sources*, 2019, **427**, 129-137.

114. *ECS Meeting Abstracts*, 2016.

115. P. Zhan, S. Wang, Y. Yuan, K. Jiao and S. Jiao, *J. Electrochem. Soc.*, 2015, **162**, A1028-A1032.

116. P. Zheng, J. Su, Y. Wang, W. Zhou, J. Song, Q. Su, N. Reeves-McLaren and S. Guo, *ChemSusChem*, 2020, **13**, 1793-1799.

117. H. Kim, D.-H. Seo, J. C. Kim, S.-H. Bo, L. Liu, T. Shi and G. Ceder, *Adv. Mater.*, 2017, **29**, 1702480.

118. S. Chong, Y. Wu, Y. Chen, S. Guo, Z. Tai, C. Shu, Q. Tan, J. Sun and Y. Liu, *Electrochim. Acta*, 2019, **293**, 299-306.

119. Y.-S. Xu, Q.-H. Zhang, D. Wang, J.-C. Gao, X.-S. Tao, Y. Liu, Y.-G. Sun, L. Gu, B.-B. Chang, C.-T. Liu, S.-Q. Shi and A.-M. Cao, *Energy Storage Mater.*, 2020, **31**, 20-26.

120. B. Lin, X. Zhu, L. Fang, X. Liu, S. Li, T. Zhai, L. Xue, Q. Guo, J. Xu and H. Xia, *Adv. Mater.*, 2019, **31**, e1900060.

121. E. Markevich, G. Salitra, Y. Talyosef, U.-H. Kim, H.-H. Ryu, Y.-K. Sun and D. Aurbach, *ACS Applied Energy Materials*, 2018, **1**, 2600-2607.

122. L. Biasi, A. Schiele, M. Roca-Ayats, G. García, T. Brezesinski, P. Hartmann and J. Janek, *ChemSusChem*, 2019, **12**.

123. H. Arai, S. Okada, Y. Sakurai and J.-i. Yamaki, *Solid State Ionics*, 1998, **109**, 295-302.

124. Z. Zhang, D. Fouchard and J. R. Rea, *J. Power Sources*, 1998, **70**, 16-20.

125. U. H. Kim, D. W. Jun, K. J. Park, Q. Zhang, P. Kaghazchi, D. Aurbach, D. T. Major, G. Goobes, M. Dixit, N. Leifer, C. M. Wang, P. Yan, D. Ahn, K. H. Kim, C. S. Yoon and Y. K. Sun, *Energy & Environmental Science*, 2018, **11**, 1271-1279.

126. M. Bianchini, M. Roca-Ayats, P. Hartmann, T. Brezesinski and J. Janek, *Angew. Chem. Int. Ed.*, 2019, **58**, 10434-10458.

127. H.-H. Ryu, G.-T. Park, C. S. Yoon and Y.-K. Sun, *Journal of Materials Chemistry A*, 2019, **7**, 18580-18588.

128. S. Miyazaki, S. Kikkawa and M. Koizumi, *Synth. Met.*, 1983, **6**, 211-217.

129. K. Park, B.-C. Yu and J. B. Goodenough, *Chem. Mater.*, 2015, **27**, 6682-6688.

130. P. Vassilaras, X. Ma, X. Li and G. Ceder, *J. Electrochem. Soc.*, 2012, **160**, A207-A211.

131. L. Wang, J. Wang, X. Zhang, Y. Ren, P. Zuo, G. Yin and J. Wang, *Nano Energy*, 2017, **34**, 215-223.

132. Y. Ono, *Electrochemistry*, 2018, **86**, 309-314.

133. R. Kaushalya, P. Iyngaran, N. Kuganathan and A. Chroneos, *Energies*, 2019, **12**, 3094.

134. G. Meligrana, W. Lueangchaichaweng, F. Colò, M. Destro, S. Fiorilli, P. Pescarmona and C. Gerbaldi, *Electrochim. Acta*, 2017, **235**.

135. D. Kitsche, S. Schweidler, A. Mazilkin, H. Geßwein, F. Fauth, E. Suard, P. Hartmann, T. Brezesinski, J. Janek and M. Bianchini, *Materials Advances*, 2020, **1**, 639-647.

136. H. Kim, D.-H. Seo, A. Urban, J. Lee, D.-H. Kwon, S.-H. Bo, T. Shi, J. K. Papp, B. D. McCloskey and G. Ceder, *Chem. Mater.*, 2018, **30**, 6532-6539.

137. T. Masese, K. Yoshii, Y. Yamaguchi, T. Okumura, Z.-D. Huang, M. Kato, K. Kubota, J. Furutani, Y. Orikasa, H. Senoh, H. Sakaebe and M. Shikano, *Nature Communications*, 2018, **9**, 3823.

138. S.-T. Myung, S. Komaba, N. Kumagai and K. Kurihara, *Chemistry Letters - CHEM LETT*, 2001, 1114-1115.

139. N. Ortiz-Vitoriano, N. E. Drewett, E. Gonzalo and T. Rojo, *Energy & Environmental Science*, 2017, **10**, 1051-1074.

140. Y.-E. Zhu, X. Qi, X. Chen, X. Zhou, X. Zhang, J. Wei, Y. Hu and Z. Zhou, *Journal of Materials Chemistry A*, 2016, **4**, 11103-11109.

141. Y. Shen, S. Birgisson and B. B. Iversen, *Journal of Materials Chemistry A*, 2016, **4**, 12281-12288.

142. X. Wang, M. Tamaru, M. Okubo and A. Yamada, *The Journal of Physical Chemistry C*, 2013, **117**, 15545-15551.

143. Z.-Y. Li, J. Zhang, R. Gao, H. Zhang, Z. Hu and X. Liu, *ACS Applied Materials & Interfaces*, 2016, **8**, 15439-15448.

144. Q.-C. Wang, E. Hu, Y. Pan, N. Xiao, F. Hong, Z.-W. Fu, X.-J. Wu, S.-M. Bak, X.-Q. Yang and Y.-N. Zhou, *Advanced Science*, 2017, **4**, 1700219.

145. J. Zhao, X. Zhang, J. Wang, X. Yang, J. Deng and Y. Wang, *J. Solid State Electrochem.*, 2020, **24**, 1349-1361.

146. Y. Wang, F. Zhao, Y. Qian and H. Ji, *ACS Applied Materials & Interfaces*, 2018, **10**, 42380-42386.

147. P. Manikandan, K. Kishor, J. Han and Y. Kim, *Journal of Materials Chemistry A*, 2018, **6**, 11012-11021.

148. H. V. Ramasamy, B. Senthilkumar, P. Barpanda and Y.-S. Lee, *Chem. Eng. J.*, 2019, **368**, 235-243.

149. J. U. Choi, J. Kim, J.-Y. Hwang, J. H. Jo, Y.-K. Sun and S.-T. Myung, *Nano Energy*, 2019, **61**, 284-294.

150. X. He, J. Wang, L. Wang and J. Li, *Materials (Basel)*, 2016, **9**.

151. X. Hu, H. Guo, W. Peng, Z. Wang, X. Li and Q. Hu, *J. Electroanal. Chem.*, 2018, **822**, 57-65.

152. S. Zhang, H. Gu, H. Pan, S. Yang, W. Du, X. Li, M. Gao, Y. Liu, M. Zhu, L. Ouyang, D. Jian and F. Pan, *Advanced Energy Materials*, 2017, **7**, 1601066.

153. J. Zhang, H. Zhang, R. Gao, Z. Li, Z. Hu and X. Liu, *Phys. Chem. Chem. Phys.*, 2016, **18**, 13322-13331.

154. J. Li, C. Zhan, J. Lu, Y. Yuan, R. Shahbazian-Yassar, X. Qiu and K. Amine, *ACS Appl. Mater. Interfaces*, 2015, **7**, 16040-16045.
155. K. J. Carroll, D. Qian, C. Fell, S. Calvin, G. M. Veith, M. Chi, L. Baggetto and Y. S. Meng, *Phys. Chem. Chem. Phys.*, 2013, **15**, 11128-11138.
156. H. Liu, D. Qian, M. G. Verde, M. Zhang, L. Baggetto, K. An, Y. Chen, K. J. Carroll, D. Lau, M. Chi, G. M. Veith and Y. S. Meng, *ACS Appl. Mater. Interfaces*, 2015, **7**, 19189-19200.
157. Z. Tai, X. Li, W. Zhu, M. Shi, Y. Xin, S. Guo, Y. Wu, Y. Chen and Y. Liu, *J. Colloid Interface Sci.*, 2020, **570**, 264-272.
158. Z.-G. Gao, K. Sun, L.-N. Cong, Y.-H. Zhang, Q. zhao, R.-S. Wang, H.-M. Xie, L.-Q. Sun and Z.-M. Su, *J. Alloys Compd.*, 2016, **654**, 257-263.
159. X.-Y. Feng, C. Shen, H.-F. Xiang, H.-K. Liu, Y.-C. Wu and C.-H. Chen, *J. Alloys Compd.*, 2017, **695**, 227-232.
160. S. H. Jung, D. H. Kim, P. Brüner, H. Lee, H. J. Hah, S. K. Kim and Y. S. Jung, *Electrochim. Acta*, 2017, **232**, 236-243.
161. N. Kiziltas-Yavuz, A. Bhaskar, D. Dixon, M. Yavuz, K. Nikolowski, L. Lu, R.-A. Eichel and H. Ehrenberg, *J. Power Sources*, 2014, **267**, 533-541.
162. Q. Pang, Q. Fu, Y. Wang, Y. Zhang, B. Zou, F. Du, G. Chen and Y. Wei, *Electrochim. Acta*, 2015, **152**, 240-248.
163. U. Nisar, R. Amin, R. Essehli, R. A. Shakoor, R. Kahraman, D. K. Kim, M. A. Khaleel and I. Belharouak, *J. Power Sources*, 2018, **396**, 774-781.
164. T. Yang, N. Zhang, Y. Lang and K. Sun, *Electrochim. Acta*, 2011, **56**, 4058-4064.
165. T. Hwang, J. K. Lee, J. Mun and W. Choi, *J. Power Sources*, 2016, **322**, 40-48.
166. J. Gao, T. Yuan, S. Luo, J. Ruan, H. Sun, J. Yang and S. Zheng, *J. Colloid Interface Sci.*, 2020, **570**, 153-162.
167. J. Li, M. Zhang, D. Zhang, Y. Yan and Z. Li, *Chem. Eng. J.*, 2020, **402**, 126195.
168. T.-F. Yi, Y. Xie, Y.-R. Zhu, R.-S. Zhu and M.-F. Ye, *J. Power Sources*, 2012, **211**, 59-65.
169. G. B. Zhong, Y. Y. Wang, Z. C. Zhang and C. H. Chen, *Electrochim. Acta*, 2011, **56**, 6554-6561.
170. P. Sun, Y. Ma, T. Zhai and H. Li, *Electrochim. Acta*, 2016, **191**, 237-246.
171. Y. Luo, T. Lu, Y. Zhang, L. Yan, S. S. Mao and J. Xie, *J. Alloys Compd.*, 2017, **703**, 289-297.
172. M.-H. Liu, H.-T. Huang, C.-M. Lin, J.-M. Chen and S.-C. Liao, *Electrochim. Acta*, 2014, **120**, 133-139.
173. R. Amin, N. Muralidharan, R. K. Petla, H. Ben Yahia, S. A. Jassim Al-Hail, R. Essehli, C. Daniel, M. A. Khaleel and I. Belharouak, *J. Power Sources*, 2020, **467**, 228318.
174. T. Risthaus, D. Zhou, X. Cao, X. He, B. Qiu, J. Wang, L. Zhang, Z. Liu, E. Paillard, G. Schumacher, M. Winter and J. Li, *J. Power Sources*, 2018, **395**, 16-24.
175. P. Hou, F. Li, Y. Wang, J. Yin and X. Xu, *Journal of Materials Chemistry A*, 2019, **7**, 4705-4713.
176. L. Wang, Y.-G. Sun, L.-L. Hu, J.-Y. Piao, J. Guo, A. Manthiram, J. Ma and A.-M. Cao, *Journal of Materials Chemistry A*, 2017, **5**, 8752-8761.
177. S. Y. Lee, J. H. Kim and Y. C. Kang, *Electrochim. Acta*, 2017, **225**, 86-92.
178. D. Yang, X.-Z. Liao, J. Shen, Y.-S. He and Z.-F. Ma, *Journal of Materials Chemistry A*, 2014, **2**, 6723-6726.
179. Y. Wen, B. Wang, G. Zeng, K. Nogita, D. Ye and L. Wang, *Chemistry – An Asian Journal*, 2015, **10**, 661-666.
180. Y. Liu, Q. Shen, X. Zhao, J. Zhang, X. Liu, T. Wang, N. Zhang, L. Jiao, J. Chen and L.-Z. Fan, *Adv. Funct. Mater.*, 2020, **30**, 1907837.
181. J. Chen, L. Li, L. Wu, Q. Yao, H. Yang, Z. Liu, L. Xia, Z. Chen, J. Duan and S. Zhong, *J. Power Sources*, 2018, **406**, 110-117.
182. Y. Wang, X. Wang, X. Li, R. Yu, M. Chen, K. Tang and X. Zhang, *Chem. Eng. J.*, 2019, **360**, 139-147.
183. H. Chen, Z. Wu, Y. Zhong, T. Chen, X. Liu, J. Qu, W. Xiang, J. Li, X. Chen, X. Guo and B. Zhong, *Electrochim. Acta*, 2019, **308**, 64-73.

184.   N. Tapia-Ruiz, W. M. Dose, N. Sharma, H. Chen, J. Heath, J. W. Somerville, U. Maitra, M. S. Islam and P. G. Bruce, *Energy & Environmental Science*, 2018, **11**, 1470-1479.

185.   J. Sun, J. Shen and T. Wang, *J. Alloys Compd.*, 2017, **709**, 481-486.

186.   Q. Zhao, Z. Guo, L. Wang, Y. Wu, F. K. Butt, Y. Zhu, X. Xu, X. Ma and C. Cao, *ACS Applied Materials & Interfaces*, 2019, **11**, 30819-30827.

187.   X. Wu, J. Guo, D. Wang, G. Zhong, M. J. McDonald and Y. Yang, *J. Power Sources*, 2015, **281**, 18-26.

188.   J.-H. Hong, M.-Y. Wang, Y.-Y. Du, L. Deng and G. He, *Journal of Materials Science: Materials in Electronics*, 2019, **30**, 4006-4013.

189.   W. Liu, T. Chen, J. Li, X. Bian, Y. Zhuo, H. Hu, J. Guo, K. Liu and J. Yan, *Solid State Ionics*, 2019, **329**, 149-154.

190.   P. Bai, K. Jiang, X. Zhang, J. Xu, S. Guo and H. Zhou, *ACS Applied Materials & Interfaces*, 2020, **12**, 10490-10495.

191.   J. H. Jo, J. U. Choi, Y. J. Park, Y. H. Jung, D. Ahn, T. Y. Jeon, H. Kim, J. Kim and S. T. Myung, *Advanced Energy Materials*, 2020, **10**, 1903605.

192.   X. Zhang, Y. Yang, X. Qu, Z. Wei, G. Sun, K. Zheng, H. Yu and F. Du, *Adv. Funct. Mater.*, 2019, **29**, 1905679.

193.   C. Jo, J. H. Jo, H. Yashiro, S.-J. Kim, Y.-K. Sun and S.-T. Myung, *Advanced Energy Materials*, 2018, **8**, 1702942.

194.   J.-Y. Hwang, J. Kim, T.-Y. Yu, H.-G. Jung, J. Kim, K.-H. Kim and Y.-K. Sun, *Journal of Materials Chemistry A*, 2019, **7**, 21362-21370.

195.   C. Tian, F. Lin and M. M. Doeff, *Acc. Chem. Res.*, 2018, **51**, 89-96.

196.   B. Huang, D. Liu, L. Zhang, K. Qian, K. Zhou, X. Cai, F. Kang and B. Li, *ACS Applied Energy Materials*, 2019, **2**, 7403-7411.

197.   H. Q. Pham, J. Lee, H. M. Jung and S.-W. Song, *Electrochim. Acta*, 2019, **317**, 711-721.

198.   K. Yoo, Y. Kang, K. Im and C. Kim, *Materials*, 2017, **10**, 1273.

199.   B. Song, W. Li, S.-M. Oh and A. Manthiram, *ACS Applied Materials & Interfaces*, 2017, **9**, 9718-9725.

200.   H. Liang, Z. Wang, H. Guo, J. Wang and J. Leng, *Appl. Surf. Sci.*, 2017, **423**, 1045-1053.

201.   D. Wang, X. Li, Z. Wang, H. Guo, Z. Huang, L. Kong and J. Ru, *J. Alloys Compd.*, 2015, **647**, 612-619.

202.   T. Tao, C. Chen, Y. Yao, B. Liang, S. Lu and Y. Chen, *Ceram. Int.*, 2017, **43**, 15173-15178.

203.   L. Yao, F. Liang, J. Jin, B. V. R. Chowdari, J. Yang and Z. Wen, *Chem. Eng. J.*, 2020, **389**, 124403.

204.   V.-C. Ho, S. Jeong, T. Yim and J. Mun, *J. Power Sources*, 2020, **450**, 227625.

205.   S.-H. Lee, G.-J. Park, S.-J. Sim, B.-S. Jin and H.-S. Kim, *J. Alloys Compd.*, 2019, **791**, 193-199.

206.   W. Cho, S.-M. Kim, J. H. Song, T. Yim, S.-G. Woo, K.-W. Lee, J.-S. Kim and Y.-J. Kim, *J. Power Sources*, 2015, **282**, 45-50.

207.   M. A. R. Khollari, M. K. Azar, M. Esmaeili, M. Tanhaei, A. Dolati and H. SeyedMortezaHosseini, *J. Alloys Compd.*, 2020, 154924.

208.   M. Zhao, Y. Xu, P. Ren, Y. Zuo, W. Su and Y. Tang, *Dalton Transactions*, 2020, **49**, 2933-2940.

209.   J.-H. Shim, Y.-M. Kim, M. Park, J. Kim and S. Lee, *ACS Applied Materials & Interfaces*, 2017, **9**, 18720-18729.

210.   L. Liang, G. Hu, F. Jiang and Y. Cao, *J. Alloys Compd.*, 2016, **657**, 570-581.

211.   S. Dai, G. Yan, L. Wang, L. Luo, Y. Li, Y. Yang, H. Liu, Y. Liu and M. Yuan, *J. Electroanal. Chem.*, 2019, **847**, 113197.

212.   J. Zhu, G. Cao, Y. Li, S. Wang, S. Deng, J. Guo, Y. Chen, T. Lei, J. Zhang and S. Chang, *Electrochim. Acta*, 2019, **325**, 134889.

213.   Y.-D. Xu, W. Xiang, Z.-G. Wu, C.-L. Xu, Y.-C. Li, X.-D. Guo, G.-P. Lv, X. Peng and B.-H. Zhong, *Electrochim. Acta*, 2018, **268**, 358-365.

214.   W. Zhang, J. Li, Y. Guan, Y. Jin, W. Zhu, X. Guo and X. Qiu, *J. Power Sources*, 2013, **243**, 661-667.

215. L. Sun, J. Wang, K. Jiang and S. Fan, *J. Power Sources*, 2014, **248**, 265-272.
216. A. Nugroho, S. J. Kim, W. Chang, K. Y. Chung and J. Kim, *J. Power Sources*, 2013, **244**, 164-169.
217. Z. Zhao, Y. Xu, M. Ji and H. Zhang, *Electrochim. Acta*, 2013, **109**, 645-650.
218. M. Ji, Y. Xu, Z. Zhao, H. Zhang, D. Liu, C. Zhao, X. Qian and C. Zhao, *J. Power Sources*, 2014, **263**, 296-303.
219. W. Wang, H. Wang, S. Wang, Y. Hu, Q. Tian and S. Jiao, *J. Power Sources*, 2013, **228**, 244-249.
220. W. Chen, S. Kuang, Z. Liu, H. Fu, Q. Yun, D. Xu, H. Hu and X. Yu, *J. Alloys Compd.*, 2020, **835**, 155327.
221. Y. Chen, Y. Zhang, B. Chen, Z. Wang and C. Lu, *J. Power Sources*, 2014, **256**, 20-27.
222. D. Zhang, Y. Liu, L. Wu, L. Feng, S. Jin, R. Zhang and M. Jin, *Electrochim. Acta*, 2019, **328**, 135086.
223. R. Du, Y. Bi, W. Yang, Z. Peng, M. Liu, Y. Liu, B. Wu, B. Yang, F. Ding and D. Wang, *Ceram. Int.*, 2015, **41**, 7133-7139.
224. Y. Jiang, Z. Liu, Y. Zhang, H. Hu, X. Teng, D. Wang, P. Gao and Y. Zhu, *Electrochim. Acta*, 2019, **309**, 74-85.
225. Z. Huang, Z. Wang, Q. Jing, H. Guo, X. Li and Z. Yang, *Electrochim. Acta*, 2016, **192**, 120-126.
226. Y. Lei, J. Ai, S. Yang, C. Lai and Q. Xu, *Journal of The Taiwan Institute of Chemical Engineers*, 2019, **97**, 255-263.
227. Y. Li, Q. Su, Q. Han, P. Li, L. Li, C. Xu, X. Cao and G. Cao, *Ceram. Int.*, 2017, **43**, 3483-3488.
228. B. Chu, S. Liu, L. You, D. Liu, T. Huang, Y. Li and A. Yu, *ACS Sustainable Chemistry & Engineering*, 2020, **8**, 3082-3090.
229. M. Zhang, H. Zhao, M. Tan, J. Liu, Y. Hu, S. Liu, X. Shu, H. Li, Q. Ran, J. Cai and X. Liu, *Journal of Alloys and Compounds*, 2019, **774**, 82-92.
230. J. Xu, X. Chen, C. Wang, L. Yang, X. Gao, Y. Zhou, K. Xiao and X. Xi, *Ceram. Int.*, 2017, **43**.
231. Q. Chen, L. Luo, L. Wang, T. Xie, S. Dai, Y. Yang, Y. Li and M. Yuan, *J. Alloys Compd.*, 2018, **735**, 1778-1786.
232. G.-T. Park, H.-H. Ryu, N.-Y. Park, C. S. Yoon and Y.-K. Sun, *J. Power Sources*, 2019, **442**, 227242.
233. G. Shang, Y. Tang, Y. Lai, J. Wu, X. Yang, H. Li, C. Peng, J. Zheng and Z. Zhang, *J. Power Sources*, 2019, **423**, 246-254.
234. Z. Gan, G. Hu, Z. Peng, Y. Cao, H. Tong and K. Du, *Appl. Surf. Sci.*, 2019, **481**, 1228-1238.
235. Y. Lv, X. Cheng, W. Qiang and B. Huang, *J. Power Sources*, 2020, **450**, 227718.
236. Z. Huang, Z. Wang, X. Zheng, H. Guo, X. Li, Q. Jing and Z. Yang, *Electrochim. Acta*, 2015, **182**, 795-802.
237. X. Liu, S. Wang, L. Wang, K. Wang, X. Wu, P. Zhou, Z. Miao, J. Zhou, Y. Zhao and S. Zhuo, *J. Power Sources*, 2019, **438**, 227017.
238. D. Yuan, W. He, F. Pei, F. Wu, Y. Wu, J. Qian, Y. Cao, X. Ai and H. Yang, *Journal of Materials Chemistry A*, 2013, **1**, 3895-3899.
239. V. S. Rangasamy, S. Thayumanasundaram, J.-P. Locquet and J. W. Seo, *Ionics*, 2017, **23**, 645-653.
240. K. Kaliyappan, W. Xiao, K. R. Adair, T.-K. Sham and X. Sun, *ACS Omega*, 2018, **3**, 8309-8316.
241. T. Y. Yu, J. Y. Hwang, D. Aurbach and Y. K. Sun, *ACS Appl. Mater. Interfaces*, 2017, **9**, 44534-44541.
242. P. Hou, Y. Sun, F. Li, Y. Sun, X. Deng, H. Zhang, X. Xu and L. Zhang, *Nanoscale*, 2019, **11**, 2787-2794.
243. J. Choi, K. H. Kim, C. H. Jung and S. H. Hong, *Chemical communications (Cambridge, England)*, 2019, **55**, 11575-11578.
244. S. Bao, S.-h. Luo, Z.-y. Wang, S.-x. Yan, Q. Wang and J.-y. Li, *J. Power Sources*, 2018, **396**, 404-411.
245. S. Bao, S. Luo, Z. Wang, Q. Wang, A. Hao, Y. Zhang and Y. Wang, *J. Power Sources*, 2017, **362**, 323-331.

246. M. Sathiya, K. Hemalatha, K. Ramesha, J. M. Tarascon and A. S. Prakash, *Chem. Mater.*, 2012, **24**, 1846-1853.
247. J.-Y. Hwang, S.-T. Myung, J. Choi, C. Yoon, H. Yashiro and Y.-K. Sun, *J. Mater. Chem. A*, 2017, **5**.
248. J. U. Choi, J. Kim, J. H. Jo, H. J. Kim, Y. H. Jung, D.-C. Ahn, Y.-K. Sun and S.-T. Myung, *Energy Storage Mater.*, 2020, **25**, 714-723.
249. C. Liu, S. Luo, H. Huang, Z. Wang, A. Hao, Y. Zhai and Z. Wang, *Electrochem. Commun.*, 2017, **82**, 150-154.
250. Q. Deng, F. Zheng, W. Zhong, Q. Pan, Y. Liu, Y. Li, G. Chen, Y. Li, C. Yang and M. Liu, *Chem. Eng. J.*, 2020, **392**, 123735.
251. S. Xu, C. Bao, M. Yu, S. Liu, L. Chen and D. Zhang, *Mater. Lett.*, 2020, **270**, 127733.
252. R. Dang, N. Li, Y. Yang, K. Wu, Q. Li, Y. L. Lee, X. Liu, Z. Hu and X. Xiao, *J. Power Sources*, 2020, **464**, 228190.
253. C.-l. Liu, S.-h. Luo, H.-b. Huang, Y.-c. Zhai and Z.-w. Wang, *Electrochim. Acta*, 2018, **286**, 114-122.
254. A. Yaroshevsky, *Geochem. Int.*, 2006, **44**, 48-55.
255. L. Mu, S. Xu, Y. Li, Y. S. Hu, H. Li, L. Chen and X. Huang, *Adv. Mater.*, 2015, **27**, 6928-6933.
256. Y. Li, Z. Yang, S. Xu, L. Mu, L. Gu, Y. S. Hu, H. Li and L. Chen, *Adv Sci (Weinh)*, 2015, **2**, 1500031.
257. Q. Li, K. Y. Fung, L. Xu, C. Wibowo and K. M. Ng, *Industrial & Engineering Chemistry Research*, 2019, **58**, 3118-3130.
258. S. Komaba, W. Murata, T. Ishikawa, N. Yabuuchi, T. Ozeki, T. Nakayama, A. Ogata, K. Gotoh and K. Fujiwara, *Adv. Funct. Mater.*, 2011, **21**, 3859-3867.
259. H. Kang, Y. Liu, K. Cao, Y. Zhao, L. Jiao, Y. Wang and H. Yuan, *Journal of Materials Chemistry A*, 2015, **3**, 17899-17913.
260. J.-Y. Hwang, S.-T. Myung and Y.-K. Sun, *Chem. Soc. Rev.*, 2017, **46**, 3529-3614.
261. C. Bommier and X. Ji, *Small*, 2018, **14**, e1703576.
262. E. Peled and S. Menkin, *J. Electrochem. Soc.*, 2017, **164**, A1703-A1719.
263. F. Wu, N. Zhu, Y. Bai, L. Liu, H. Zhou and C. Wu, *ACS Applied Materials & Interfaces*, 2016, **8**, 21381-21386.
264. A. Ponrouch, D. Monti, A. Boschin, B. Steen, P. Johansson and M. R. Palacín, *Journal of Materials Chemistry A*, 2015, **3**, 22-42.
265. T. Hosaka, K. Kubota, A. S. Hameed and S. Komaba, *Chem. Rev.*, 2020, **120**, 6358-6466.